ABSTRACT

PURSER, MOLLY FERRIS. Development and Experimental Evaluation of a Novel Annuloplasty Ring with a Shape Memory Alloy Core. (Under the direction of Dr. Denis Cormier and Dr. Gregory Buckner).

A novel annuloplasty ring with a shape memory alloy core has been developed to facilitate minimally invasive mitral valve repair. In its activated (austenitic) phase, this prototype ring provides comparable mechanical properties as commercial semi-rigid rings. In its pre-activated (martensitic) phase, this ring is flexible enough to be introduced through an 8 mm trocar and easily manipulated with robotic instruments within the confines of a left atrial model. The core is constructed of 0.508 mm diameter NiTi, which is maintained below its M_s temperature (24 °C) during deployment and suturing. After suturing, the stiffener is heated to its A_f temperature (37 °C, normal human body temperature) enabling the NiTi to retain its optimal geometry and stiffness characteristics indefinitely. The NiTi core is shape set in a furnace to the appropriate size and optimal geometry during fabrication. The ring is cooled in a saline bath prior to surgery, making it compliant and easy to manipulate. Evaluation of the ring included mechanical testing, robotic evaluation, static pressure testing, dynamic flow testing and fatigue testing. Experimental results suggest that the NiTi core ring could be a viable alternative to flexible bands in robot-assisted mitral valve repair.

Development and Experimental Evaluation of a Novel Annuloplasty Ring with a Shape Memory Alloy Core

by
Molly Ferris Purser

A dissertation submitted to the Graduate Faculty of
North Carolina State University
in partial fulfillment of the
requirements for the Degree of
Doctor of Philosophy

Industrial Engineering

Raleigh, North Carolina

2009

APPROVED BY:

_____	_____
Dr. Denis Cormier	Dr. Gregory Buckner
Co-Chair of Advisory Committee	Co-Chair of Advisory Committee
_____	_____
Dr. Ola Harrysson	Dr. Russell King

BIOGRAPHY

Molly Ferris Purser was born Molly Ann Ferris in Pittsburgh, PA. She graduated from the University of Pittsburgh with a B.S. in Industrial Engineering. She went to work for AMP, Inc. in Greensboro, NC after graduation. While working at AMP she attended the University of North Carolina at Greensboro at night and completed her M.B.A. degree. She married Lee Purser, in October 1992. After commuting to Greensboro from Burlington for a year, she finally decided it was time to find a job closer to Lee's job at MTS, Inc. in Cary, NC. They moved to Durham and Molly began working at GKN Automotive in Roxboro. Their first daughter was born a year later. Molly quit her job at GKN to stay home with their daughter. She went back to work part time at GKN a year later and work for two years until their second daughter was born. Molly again decided to stay home full-time with their two beautiful girls. After their youngest daughter started kindergarten she decided to take a class at NC State University to sharpen her skills before returning to the workforce. She had a wonderful professor, Dr. Hodgson, and realized that what she really wanted was to go back to school full-time. With the encouragement of her wonderful husband she decided to pursue a PhD in Industrial Engineering. She become interested in biomedical manufacturing and materials and decided to get a minor in Biomedical Engineering as well. The road from engineer, to mom, to PhD has been a wonderful journey.

TABLE OF CONTENTS

List of Tables..... vi
List of Figures.....vii

Chapter 1 Introduction 1

1.1 Mitral Valve Repair 1
1.2 The Annuloplasty Ring..... 3
1.2.2 Rigid Rings..... 4
1.2.3 Flexible Rings..... 6
1.2.4 Semi-Rigid Rings 7
1.3 Surgical Procedure 9
1.3.1 Conventional Surgical Access..... 9
1.3.2 Evolution Toward Minimally Invasive Surgical Access 10
1.3.3 Minimally Invasive Mitral Valve Repair..... 14
1.4 Research Objectives..... 15
1.5 Organization of Dissertation..... 16

Chapter 2 SMAC Ring Design 18

2.1 Design Parameters..... 18
2.2 NiTi Core..... 19
2.2.2 Comparison of Core Materials..... 22
2.2.3 Fabrication Process..... 23
2.2.4 Shape Setting..... 24
2.2.5 Adjusting A_f Temperature..... 26
2.2.6 Fatigue Properties..... 29
2.3 Silicone Sheathing..... 36
2.4 Sewing Cuff 37

2.5 Preliminary Evaluations 38
2.5.1 Trocar Insertion 38
2.5.2 Surgical Evaluations 41
Chapter 3 Methods and Materials 43
3.1 Mechanical Testing 43
3.2 Static Pressure Evaluations 45
3.3 Dynamic Flow Testing 47
3.4 Fatigue Testing 50
3.5 Robotic Manipulation 53
Chapter 4 Results 57
4.1 Mechanical Testing 57
4.2 Static Pressure Testing 57
4.3 Dynamic Flow Testing 59
4.4 Fatigue Testing 67
4.4.2 Confirmation of A_f temperature 70
4.5 Robotic Manipulation 70
Chapter 5 Discussion and Conclusion 75
5.1 Mechanical Testing 75
5.2 Static Pressure Testing 75
5.3 Dynamic Flow Testing 76
5.4 Fatigue Testing 77
5.5 Robotic Manipulation 77
5.6 Limitations 78
5.7 Conclusions 79
Chapter 6 Future Research 81
6.1 Animal Testing 81
6.2 FDA 510(k) Guidance 84

6.2.1 Biocompatibility 85
6.2.2 Structural Analysis..... 85
6.2.3 Suture Pull-out Tests..... 86
6.2.4 Sterilization Validation..... 86
6.2.5 Bioburden and Pyrogen testing 87
6.2.6 Shelf-life validation 87
6.3 Summary 88
References……...89

LIST OF TABLES

Table 2.1 Comparison of annuloplasty core materials 23

Table 2.2 Composition of NiTi as supplied. 24

Table 2.3 CG Future® band adverse incidents reported to FDA in MAUDE in which there was a fracture of the core, from 2005-2008. 32

Table 3.1 Material Properties of NiTi wire core used for ANSYS model (TiNi Alloy Company) 52

Table 3.2 Robotic evaluation trials indicating various suture methods 56

Table 4.1 Static flow testing results from three individual explanted porcine hearts. Regurgitation is the backflow through the mitral valve. 58

Table 4.2 Regurgitant fraction for each heart at low and high peak left ventricular pressure. Percent regurgitant fraction is shown for both the failed valve (FRF) and the repaired valve (RRF), all hears had a decrease in MR after repair. 61

Table 4.3 ANOVA table for mixed model for RRF (repaired regurgitant fraction), the main source of error in the model is due to FRF and the random heart effect variables. 65

LIST OF FIGURES

Figure 1.1 (a) Front view of heart (National Library of Medicine and the National Institutes of Health Medline Plus Medical Encyclopedia, 2008b) (b) cut away view showing location of mitral valve (National Library of Medicine and the National Institutes of Health Medline Plus Medical Encyclopedia, 2008a) 2

Figure 1.2 Mitral valve regurgitation (National Library of Medicine and the National Institutes of Health Medline Plus Medical Encyclopedia, 2006) 2

Figure 1.3 Repair of mitral valve with annuloplasty ring (A. Carpentier, 2007) 4

Figure 1.4 Carpentier-Edwards Classic Annuloplasty Ring (Edwards Lifesciences, LLC, Irvine, CA) contains a solid titanium core..... 5

Figure 1.5 Commercial flexible bands and rings: (a) SJM Tailor® Flexible Ring+Band (St. Jude Medical, Inc., St. Paul, MN), (b) Duran AnCore® Ring and Band System (Medtronic, Inc., Minneapolis, MN), (c) Cosgrove-Edwards Annuloplasty System (Edwards Lifesciences LLC, Irvine, CA) 7

Figure 1.6 Commercially available semi-rigid rings: (a) SJM® Séguin Ring (St. Jude Medical Inc., St. Paul, MN), (b) CG Future® (Medtronic, Inc., Minneapolis, MN), (c) Carpentier-Edwards Physio Ring (Edwards Lifesciences LLC, Irvine, CA) 8

Figure 1.7 (a) da Vinci Robot surgical console (b) Surgeon at console at the Intuitive Surgical Inc. training center, Sunnyvale, CA 12

Figure 1.8 (a) Robotic arm with surgical tools and endoscope (in center). (b) End effectors with various surgical tools which mount to robot arms. 13

Figure 1.9 Patient preparation for robotic mitral valve repair surgery. (Tatooles, Pappas, Gordon, & Slaughter, 2004)..... 15

Figure 2.1 (a) Ring at 24°C (martensitic phase) is easily straightened; (b-c) changes in shape during heating; (d) ring at 37°C (austenitic phase) in final shape 20

Figure 2.2 ANSYS nodal output model of a Physio ring - response to a 2.0 mm applied displacement 21

Figure 2.3 Simulated and experimental force versus displacement data for the ANSYS model and actual Physio ring. 22

Figure 2.4 Mandrel used for shape setting wire core into three-dimensional saddle shape. 25

Figure 2.5 Stainless steel pin and plate fixture used to shape set wire core, three fixtures were fabricated one for each ring size: 26 mm, 28mm, and 30 mm. 26

Figure 2.6 Position of ring for A_f confirmation, ring was compressed 4 mm in the anteroposterior direction with a square mandrel on a universal testing machine. 28

Figure 2.7 A_f temperature confirmation, displacement of 4 mm at increasing temperature, after 37°C the required force stabilizes, corresponding to the A_f temperature. 29

Figure 2.8 Magnification (2x) of the Physio ring on the left and the SJM® ring on the right showing variations in the polyester knit of the Physio versus the weft knit of the SJM® ring. 37

Figure 2.9 Magnification (2x) of SMAC sewing cuff materials. (A) nylon knit material, (B) circular braided polyester 38

Figure 2.10 (a) Set up of da Vinci Surgical Robot with two robot arms with 8 mm trocars, and one arm with the endoscope. (b) End effector attached to robotic arm, passes through the 8 mm trocar. 39

Figure 2.11 (a – d) SMAC ring straightened and deployed through 8 mm trocar with the robotic end effector 40

Figure 2.12 (a) and (b) Semi -rigid Physio ring cannot be inserted through the 8 mm trocar. 41

Figure 2.13 Surgical evaluations using the da Vinci Surgical System: (a) SMAC ring being deployed through an 8 mm trocar, (b) ring being manipulated and secured using robotic instruments. 42

Figure 2.14 (a) Robotic tools manipulated ring easily before activation. (b) SMAC ring sutured into explanted bovine heart and activated through Joule heating 42

Figure 3.1 Photograph of the universal testing machine used for temperature-controlled experiments 44

Figure 3.2 Photograph of the temperature-controlled water bath. Ring is compressed in anterior-posterior direction by the mandrel..... 45

Figure 3.3 (a) Explanted porcine heart with left atrium removed, in fixture for static pressure testing. Static column of saline provides back pressure on mitral valve. (b) Ring sutured into porcine heart and active by Joule heating, wires connected to a power supply 46

Figure 3.4 Explanted porcine heart connected to the left pulse duplication system. (Richards et al., 2009) 48

Figure 3.5 (a) Leaflet repair after triangular resection using running monofilament suture, arrow indicates repair. (b) Physio ring inserted into using parachute technique 49

Figure 3.6 Static pressure check before closing atriotomy: (a) SMAC ring, 26 mm (b) Physio ring, 26 mm..... 50

Figure 3.7 Endoscopic pictures during dynamic flow testing. (a) and (d) Normal mitral valve, (b) and (e) Valve after mitral regurgitation has been induced, arrow indicates flail leaflet. (c) Repaired valve with the SMAC ring. (f) Repaired valve with the Physio ring. 51

Figure 3.8 Fatigue testing apparatus, ring and fixtures are in water bath 54

Figure 3.9 Solid model of fatigue testing set up, anterior of ring is held fixed; posterior is displaced 4 mm per cycle at rate of 2 Hz. 54

Figure 3.10 Set up for robotic evaluation with porcine heart placed in fixture. The da Vinci Surgical robot with two robot arms and endoscope attached. Surgeon seated at console. 55

Figure 4.1 Compression test results for commercial rings and SMAC ring (37°C and 24°C). 58

Figure 4.2 Mitral regurgitation of failed valve and repaired valve for each of the static flow trials..... 59

Figure 4.3 Regurgitant fraction for the output at both high and low left ventricular pressure for the Physio and the SMAC ring. The variability of the FRF is much greater than the variability of the RRF. 62

Figure 4.4 Baseline output per stroke per heart, (a) peak ventricular pressure 120 mm Hg, (b) peak ventricular pressure 150 mm Hg. Hearts that were randomly assigned the Physio ring had a lower baseline output measurement than hearts assigned the SMAC ring due to the natural size variation. 64

Figure 4.5 Residual plot data points are randomly distributed, therefore do not indicate any inhomogeneity of variance or non-normality of the RRF model 66

Figure 4.6 Actual versus predicted plot for the MIXED model for the RRF. 66

Figure 4.7 Two periods of fatigue test data: Cycle 1 versus Cycle 1.9 million 67

Figure 4.8 Several periods of force data over course of fatigue testing. 68

Figure 4.9 Maximum (tension) and minimum (compression) and mean force data over the 1.9 million cycles. 68

Figure 4.10 NiTi wire core before fatigue testing (280x magnification): (a) posterior section, (b) at trigone (maximum bend radius). Only surface oxidation and small surface scratches present 69

Figure 4.11 NiTi wire core after fatigue testing: (a) at 70x magnification showing silicone sheathing and wire core, (b) at 280x magnification showing maximum bend radius. 70

Figure 4.12 Robotic evaluation with SMAC ring, mitral annulus overlaid with dotted line. Half sutures in place, ring can be moved for visualization of annulus. 71

Figure 4.13 SMAC ring with only one stitch remaining, annulus is overlaid by dotted line. 71

Figure 4.14 Robotic evaluation with Physio ring (Trial 3), dotted line shows the mitral annulus, arrows indicate areas of excessive stress on tissue and suture after 4th suture. 72

Figure 4.15 Physio ring with half of the sutures in place, dotted line outlines annulus, arrows indicate tissue deformation and stress on sutures. 73

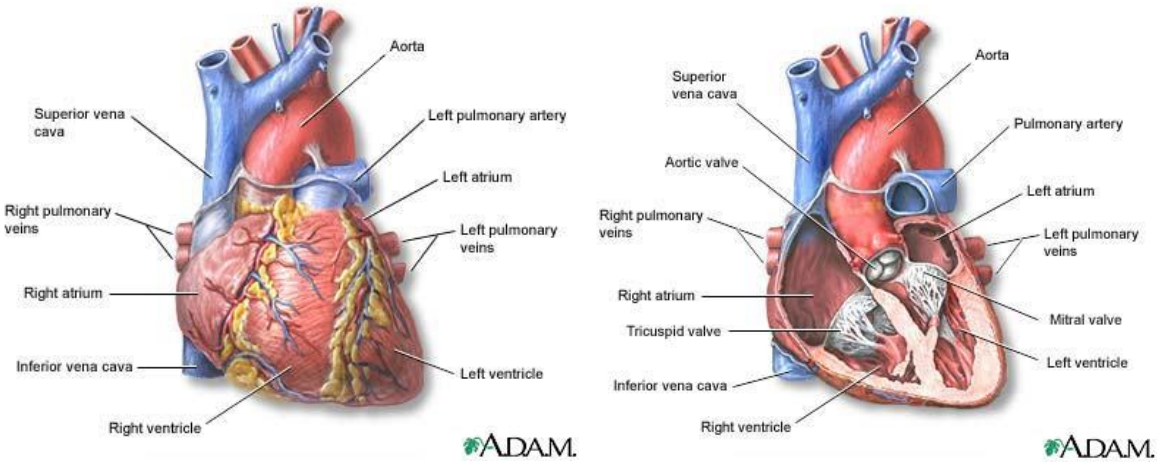
Figure 4.16 Physio ring with two more sutures to be placed, dotted line outlines annulus, arrows indicated un-knotted sutures. 73

Chapter 1 Introduction

1.1 *Mitral Valve Repair*

Mitral valve regurgitation (MVR) occurs when the mitral valve, which is located between the left atrium and left ventricle, does not close properly during systole thereby allowing a residual amount of blood to flow back into the left atrium instead of through the aorta to the body, Figure 1.1 and Figure 1.2. Mitral valve prolapse, which often leads to MVR, is estimated to occur in 1.6% – 2.4% of the adult population (Pellerin, Brecker, & Veyrat, 2002; Gillinov et al., 1998). MVR is one of the leading causes of cardiovascular disorders requiring surgery (Pellerin et al., 2002). Other causes of MVR include Barlow's disease (a thickening of the mitral leaflets), rheumatic fever (a complication of strep throat infections), endocarditis (infection of the inner lining of the heart), ischemic mitral valve prolapse (caused by complete or partial blockage of one or more of the coronary arteries due to coronary artery disease), and congenital defects.

Mitral valve repair is preferred over mitral valve replacement because of excellent long term survival, durability of the repair and freedom from long term anticoagulant drug therapy associated with valve replacement (Spiegelstein et al., 2007). In a study investigating the durability of mitral valve repair, Gillinov et al. (1998) found that 92.9% of the patients with degenerative MVR did not have to



(a) (b)

Figure 1.1 (a) Front view of heart (National Library of Medicine and the National Institutes of Health Medline Plus Medical Encyclopedia, 2008b) (b) cut away view showing location of mitral valve (National Library of Medicine and the National Institutes of Health Medline Plus Medical Encyclopedia, 2008a)

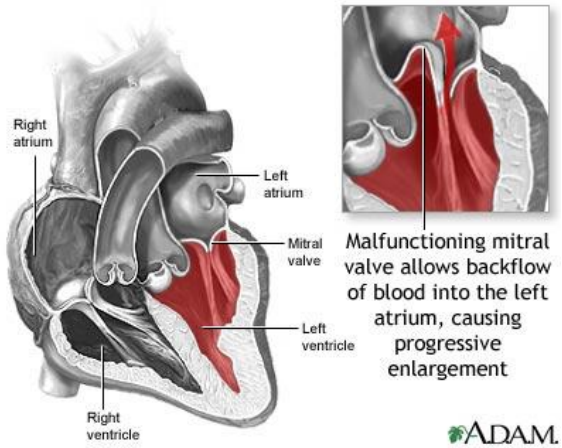


Figure 1.2 Mitral valve regurgitation (National Library of Medicine and the National Institutes of Health Medline Plus Medical Encyclopedia, 2006)

undergo re-operation surgery within 10 years (N=1072 patients). Surgical repair techniques include annuloplasty, posterior leaflet resection, posterior sliding repair, chordal transfer, chordal shortening and calcium debridement (Gillinov et al., 1998). A critical component of mitral valve repair is the annuloplasty ring: a full ring or partial band that is sutured around the annulus to provide support and minimize stress on the valve, Figure 1.3 (Gillinov et al., 1998).

1.2 *The Annuloplasty Ring*

Dr. Alain Carpentier developed the first rigid annuloplasty ring in the late 1960's (Duran, 1999). Along with this ring came the first standard surgical procedure for mitral valve repair using a permanently implanted ring that stabilized the annulus. Subsequent experiments and clinical echocardiograph data showed that the mitral valve annulus continually changed size and shape during the cardiac cycle (Flachskampf et al., 2000; Kaplan et al., 2000). This led Dr. Carlos Duran to develop a flexible ring that could conform to the changing annulus (Duran, 1999) . Thus began the continued controversy on the optimal mechanical properties of the annuloplasty ring. Today, there are many different annuloplasty rings and bands of varying shape and stiffness, each claiming to be better than the others. The types of rings can be broadly categorized as rigid, flexible and semi-rigid.

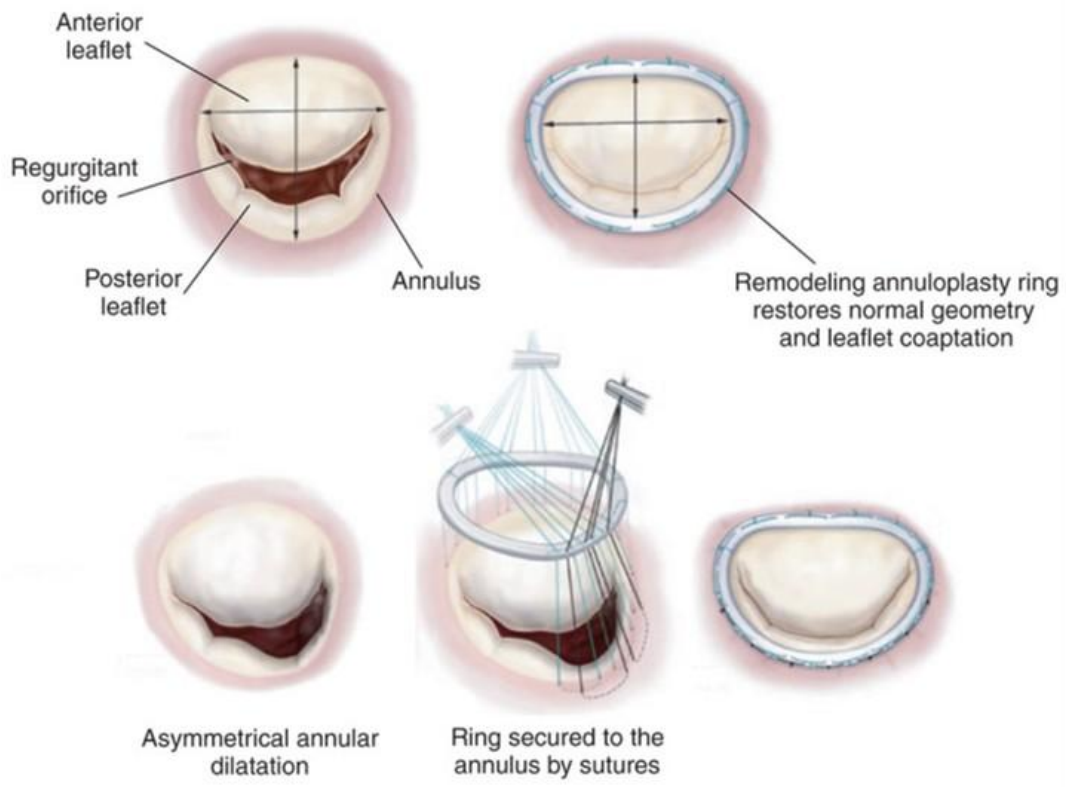


Figure 1.3 Repair of mitral valve with annuloplasty ring (Carpentier, 2007)

1.2.2 Rigid Rings

Rigid rings have a solid titanium core enabling aggressive remodeling of the annulus. However, the rigidity of the rings has been shown to decrease natural annular motion during the cardiac cycle (Sharony et al., 2004). The Carpentier-Edwards Classic Ring (Edwards Lifesciences, Irvine, CA) is one example of a rigid ring; this ring has been used successfully for over 30 years, Figure 1.4 (Rubenstein, Reichart, & Letsou, 2001). Rigid rings support the mitral annulus and immobilize the

posterior portion in a horizontal plane, thereby maintaining a theoretically optimal orifice area (Rubenstein et al., 2001).



Figure 1.4 Carpentier-Edwards Classic Annuloplasty Ring (Edwards Lifesciences, LLC, Irvine, CA) contains a solid titanium core.

As transesophageal and three-dimensional echocardiograms developed over the past three decades, it was found that the mitral annulus is in constant motion with the cardiac cycle. The annulus flexes toward the left ventricle apex during systole, and the posterior moves toward the anterior portion as the mitral annulus becomes more elliptical (Flachskampf et al., 2000; Rubenstein et al., 2001). The largest movement is in the posterior portion which is attached to the muscular portion of the heart allowing it to contract and shorten, resulting in a 25-40% reduction of the mitral valve annulus (Rubenstein et al., 2001). Flexible rings were introduced to address the limitation of rigid rings to eliminate the natural motion of the mitral annulus.

1.2.3 Flexible Rings

Flexible rings and bands are comprised of a polyester sewing cuff with a flexible silicone core, Figure 1.5. The SJM Tailor® Flexible Ring + Band (St. Jude Medical Incorporated, St. Paul, MN) is a full ring that can be cut into a partial band for use in both mitral and tricuspid valve repair. Even though flexible rings were designed to allow natural motion of the mitral annulus, this technology has been the subject of continued controversy. Dagum et al. (2001) placed radiopaque markers around the mitral valves of sheep divided into three groups: flexible full rings, flexible partial bands, and a no-ring group. Cinefluoroscopy showed that both the flexible partial band and full ring fix the annulus size during the cardiac cycle. However, the partial band allowed for the three-dimensional movement of the mitral valve annulus better than full rings (Dagum et al., 2001). It was noted that incidences of repair failure are similar between semi-rigid and flexible rings, which suggests that the stiffness of the ring alone may not have a significant clinical advantage (Dagum et al., 2001). Several other researchers have shown that flexible rings do allow for more natural motion of the mitral annulus, improved end-diastolic diameter, and improved left ventricle volume output (Cosgrove et al., 1995; David, Komeda, Pollick, & Burns, 1989; Okada, Shomura, Yamaura, & Yoshikawa, 1995). The disadvantage of flexible rings is that they reportedly do not provide as much annular remodeling and stability as rigid rings (Fasol, Meinhart, Deutsch, & Binder, 2004).



(a) (b) (c)

Figure 1.5 Commercial flexible bands and rings: (a) SJM Tailor® Flexible Ring+Band (St. Jude Medical, Inc., St. Paul, MN), (b) Duran AnCore® Ring and Band System (Medtronic, Inc., Minneapolis, MN), (c) Cosgrove-Edwards Annuloplasty System, shown with handle (Edwards Lifesciences LLC, Irvine, CA)

1.2.4 Semi-Rigid Rings

Semi-rigid rings were developed to have flexibility along the anteroposterior axis, while being rigid along the transverse axis. This allows these rings to flex with the natural movement while providing support for the annulus (Fasol et al., 2004; Sharony et al., 2004). The semi-rigid rings usually contain a metal core. The CG Future® (Medtronic, Inc., Minneapolis, MN) band and the Carpentier-Edwards Physio Ring (Edwards Lifesciences,LLC, Irvine, CA) both contain a Co-Cr-Ni-Mo core. The SJM® Séguin semi-rigid ring (St. Jude Medical, Inc.,St. Paul, MN) has a solid UHMWPE inner core. Sorin Biomedica Cardio received FDA approved in February 2007 for a semi-rigid ring, the MEMO 3D, (Sorin Biomedica Cardio S.R.L., Saluggia (Vercelli), IT) which has a NiTi core that has a structure similar to a stent. Clinical trials in the U.S. began in February 2008, and will be conducted at Penn

Presbyterian Medical Center and several other US centers (U.S. National Institutes of Health, 2008). All of these core materials provide excellent corrosion resistance, good ductility, high tensile strength and toughness. The semi-rigid rings not only are selectively flexible, but are saddle shaped to conform to the natural shape of the annulus, Figure 1.6. Several research centers have shown excellent outcomes with semi-rigid rings (Raffoul et al., 1998; Seguin, Demaria, Rogier, & Chaptal, 1996; Sharony et al., 2004).



(a) (b) (c)

Figure 1.6 Commercially available semi-rigid rings: (a) SJM® Séguin Ring (St. Jude Medical Inc., St. Paul, MN) (b) CG Future® (Medtronic, Inc., Minneapolis, MN), (c) Carpentier-Edwards Physio Ring (Edwards Lifesciences LLC, Irvine, CA)

1.3 *Surgical Procedure*

1.3.1 Conventional Surgical Access

Surgical access to the mitral valve is limited by its location between the left atrium and the left ventricle. The conventional surgical procedure is via a median sternotomy, which involves a 25-30 cm incision and splitting of the sternum, allowing complete exposure and access to the heart (Glower et al., 1998). The midline incision extends from the sterna notch to the xiphoid process. The incision extends through the subcutaneous tissue to the pectoralis muscles and creates a thick flap, which is retracted. Electrocauterization is used to control bleeding. The sternum is divided with a reciprocating sternal saw, and the underlying structures are cut away from the sternum. A sternal retractor is used to separate the sternum in an upward direction, which prevents damage to the right ventricle, to provide access to the heart. The ascending aorta, inferior and superior venae cavae are cannulated and cardiopulmonary bypass (CPB) is started. The ascending aorta is clamped, cold-blood cardioplegia is initiated, and the heart is arrested. An incision is made in the left atrium (atriotomy) to gain access to the mitral valve. After the mitral valve repair, the sternum is closed with wires and the incision is closed (L. H. Cohn & Edmunds, 2007). The patient is removed from CPB and the heart is restarted.

Due to the surgical trauma of this conventional “open chest” procedure, patients generally do not return to normal activity until nine weeks post operatively

(Glower et al., 1998). Complications from medial sternotomy include dehiscence of the sternum, mediastinitis (chest infection) and osteomyelitis (bone infection) (Goodman, Kay, Teplick, & Mundth, 1983). Although complications are rare, 0.2% to 5% of patients, they are associated with increased hospital stays, increased cost and a high mortality rate (Losanoff, Richman, & Jones, 2002). In patients with deep chest infections, the mortality rate exceeds 70% (Goodman et al., 1983).

1.3.2 Evolution Toward Minimally Invasive Surgical Access

In the mid 1990's, progressive surgeons such as Cosgrove, Cohn and colleagues began to realize that the standard median sternotomy could be modified to a more minimally invasive technique (Felger, Chitwood, Nifong, & Holbert, 2001). Advances in closed-chest cardiopulmonary bypass, myocardial protection, video assisted three dimensional visualization and robotic instruments led to effective minimally invasive procedures for mitral valve repair (A. P. Kypson & Chitwood, 2004). However, many surgeons were reluctant to accept minimally invasive procedures because of the documented success and familiarity with conventional "open" procedures (Felger et al., 2001). Nevertheless, preliminary results from minimally invasive procedures showed promise, and research continued. A clinical trial at Duke University by Glower et al. (1988) was one of the first to show a side by side comparison of minimally invasive versus conventional mitral valve repair (Glower et al., 1998). Although the aortic clamp time, cardiopulmonary bypass time,

surgical procedure time and total operation room time were all longer with the minimally invasive procedure, incision size was reduced from 26 cm to only 8 cm (Glower et al., 1998). This reduced incision size resulted in a reduction of pain duration and return to normal activity in an average of only four weeks as opposed to nine weeks for the conventional open chest patients (Glower et al., 1998).

In 1998, Carpentier and colleagues used an early prototype of the da Vinci Surgical System (Intuitive Surgical, Inc. Sunnyvale, CA) to perform the first endoscopic robotically assisted mitral valve repair (A. P. Kypson & Chitwood, 2004). The da Vinci robotic system consists of a console where the operating surgeon controls the surgical robotic tools by manipulating the micro wrist instruments, Figure 1.7. The advantages of the robot system include improved maneuverability of the micro wrists (which can rotate 360°), finer movements, the elimination of tremors, (A. P. Kypson & Chitwood, 2004) and an endoscope with two small cameras positioned at an angle to allow for three-dimensional visualization of the operating field (Ballantyne, 2002 ; A. P. Kypson & Chitwood, 2004). The robotic arms have different interchangeable end effectors to facilitate cutting or grabbing (A. P. Kypson & Chitwood, 2004), Figure 1.8.

In 2000, Chitwood and colleagues began the first US FDA clinical trials using the da Vinci Surgical Robot System for mitral valve repair (A. P. Kypson & Chitwood, 2004). Results from these clinical trials (N=20) were promising: reduced incision

size resulted in decreased pain duration, decreased average hospital stay (to only 4 days), and fewer infections (A. P. Kypson & Chitwood, 2004). However, operating times were still above the four hours normally associated with conventional mitral valve repair (A. P. Kypson & Chitwood, 2004). In 2002, a multicenter Phase II FDA clinical trial was completed that included 112 patients at surgical centers throughout the United States (A. P. Kypson & Chitwood, 2004). Results showed that multiple surgical teams could duplicate the success of the first trial and all centers reported



(a) (b)

Figure 1.7 (a) da Vinci Robot surgical console (b) Surgeon at console at the Intuitive Surgical Inc. training center, Sunnyvale, CA

reductions of surgery times with increased experience (A. P. Kypson & Chitwood, 2004). In November 2002, the FDA approved the da Vinci Surgical System for use

in mitral valve repairs (A. P. Kypson & Chitwood, 2004). Patients had less scarring, decreased pain levels, fewer complications, decreased hospital stays and were able to return to normal activity levels sooner (L. H. Cohn et al., 1997). Incision size was reduced to 5 cm, and hospital stays were shortened from 9 weeks to 4 weeks (L. H. Cohn et al., 1997; Glower et al., 1998) . Disadvantages of the robotic surgery procedure compared to the conventional procedure included decreased maneuverability, reduced access and visualization, and steeper surgical learning curves (Felger et al., 2001). From an economic point of view, there was a cost



(a) (b)

Figure 1.8 (a) Robotic arm with surgical tools and endoscope (in center). (b) End effectors with various surgical tools which mount to robot arms.

savings due to the decreased hospital stay, however, this was somewhat offset by the increased capital expense of the robot as well as increased operating costs, service contracts and disposable items used in robotic surgery (L. H. Cohn et al., 1997).

1.3.3 Minimally Invasive Mitral Valve Repair

The minimally invasive procedure is similar in the beginning stages to the conventional procedure. The patient is anesthetized, and then placed with the right arm tucked at the side or above the head with the chest elevated 30 degrees. Unlike the conventional “open-chest” procedure, the heart is accessed through the right jugular vein and the femoral artery and vein. These are cannulated using transesophageal echocardiography and/or fluoroscopy and CPB is initiated with the body temperature between 26°C - 32°C. The heart is arrested with cold-blood cardioplegia given through a femoral artery cannula. A working port access in the chest is entered through a 4-5 cm incision in the fourth intercostal space in the chest (Figure 1.9). The incision is used for the video camera as well as for patient side surgical access for needle and suture retrieval and to pass the annuloplasty ring.

The mitral valve is accessed via a left atriotomy (a 3 to 4 cm incision in the left atrium). Small stab incisions for the right robotic arm are made in the fifth intercostal space parallel to the right inferior pulmonary vein. The left incision for the left robotic arm is placed 6 cm cephalad and medial to the right arm. This allows for optimal access without the robotic arms interfering with each other. The aorta is cross-clamped with an incision in the third intercostal space, and the atrium is retracted with a similar small incision on the left side. Generally a flexible ring is used in conjunction with other repair techniques such as chordal shortening or replacement,

papillary muscle reconstruction, leaflet resection and leaflet repair. Individually knotted sutures or U-clips™ (Coalescent Surgical Inc., Sunnyvale, CA) are used to secure the ring to the annulus. Standard de-airing and weaning off by-pass are completed (A. P. Kypson, 2003). Patients generally return for a follow up transthoracic echocardiogram in one month (A. P. Kypson, 2003).

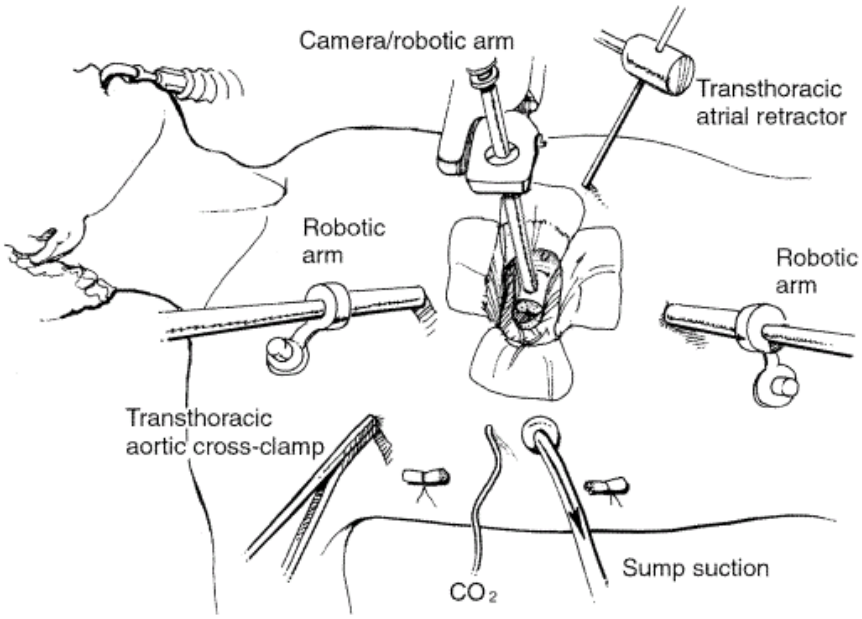


Figure 1.9 Patient preparation for robotic mitral valve repair surgery. (Tatooles, Pappas, Gordon, & Slaughter, 2004)

1.4 *Research Objectives*

The evolution of minimally invasive mitral valve repair is toward totally endoscopic surgery (Felger et al., 2001). One of the current limitations is the

difficulty in deploying rigid or semi-rigid annuloplasty rings through 8mm diameter ports known as trocars. Furthermore, rigid and semi-rigid rings are difficult to manipulate with robotic instruments within the confines of the left atrium; therefore, completely flexible rings are generally used (Felger et al., 2001; A. P. Kypson & Chitwood, 2004; Tatooles et al., 2004). In order to provide an annuloplasty ring that is flexible enough to be deployed through a trocar, yet stiff enough to provide the benefits of a semi-rigid ring, a prototype two-phase ring with a NiTi shape memory alloy core (SMAC) ring has been developed. The NiTi core remains flexible in its martensitic state for deployment, placement and suturing. The transformation to the austenitic phase takes place at body temperature, thus providing the final desired mechanical properties.

1.5 *Organization of Dissertation*

This dissertation is organized into the following sections: the design and fabrication process, testing methods and materials, results, discussion and conclusion and future research. Chapter 2 discusses the design criteria, the components of the ring, as well as the fabrication process of the NiTi core. The methods and materials of the experimental evaluations of the SMAC ring are discussed in Chapter 3. The evaluations include: mechanical, static pressure, dynamic flow and fatigue testing. A qualitative robotic manipulation surgical assessment is also presented. In Chapter 4, the results of the evaluations are

presented. Chapter 5 is a conclusion and discussion of the results as well as surgical assessment of the SMAC ring. Chapter 5 also includes a discussion of the limitations of the current research. Future research and evaluation testing is presented in Chapter 6.

Chapter 2 SMAC Ring Design

2.1 *Design Parameters*

A prototype ring was fabricated from three main components: a NiTi wire core, a silicone sheath and a polyester sewing cuff. Unlike other semi-rigid rings, which have a cobalt alloy or ultra high molecular weight polyethylene (UHMWPE) core, the NiTi core takes advantage of NiTi's excellent corrosive properties, low cytotoxicity response, MRI compatibility and unique shape memory characteristics. NiTi has been used extensively in other medical devices including stents, vena cava filters and angioplasty guide wires (Es-Souni, Es-Souni, & Fischer-Brandies, 2005). These devices, however, utilize only the super-elastic properties of NiTi; the SMAC ring utilizes the temperature-dependent shape memory effect.

The mechanical properties of the activated ring (the NiTi core in its austenitic phase) were designed to match those of commercially available semi-rigid rings. Two semi-rigid rings were targeted for comparison: the Carpentier Edwards Physio (Edwards Lifesciences LLC, Irvine, CA) and the SJM® Séguin (St. Jude Medical Inc., St. Paul, MN). Full rings were selected for comparison (rather than partial bands) because they provide additional support to the anterior portion of the mitral valve, thereby preserving the normal anterior-posterior dimension. The success of

these semi-rigid rings in mitral valve repair has been well documented (Fasol et al., 2004; Salgo et al., 2002; Sharony et al., 2004).

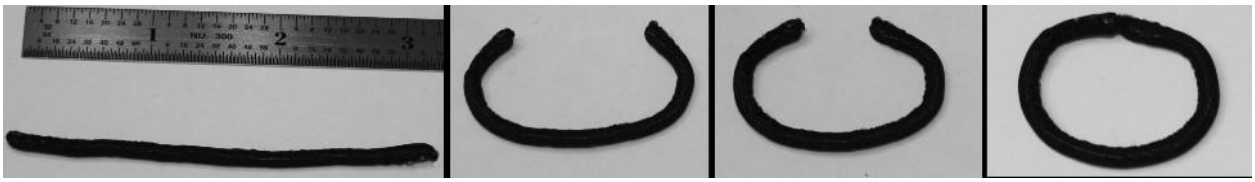
The critical design parameters for the SMAC ring are the NiTi activation temperatures. The martensite start temperature (M_s) must be below 27°C to enable the ring to be flexible enough to be introduced through an 8 mm trocar and easily manipulated within the heart. The austenite finish temperature (A_f) must be normal body temperature (37°C) in order for the ring to retain the desired mechanical properties and its optimal shape *in vivo*. Other important design considerations are related to the sheathing and cuff materials. The sheathing must provide compliant support for the core. It must be biocompatible, and thus must not contain plasticizers which might contain phthalate additives. The sewing cuff will be in direct contact with surrounding heart tissue; therefore it must be biocompatible, durable and resilient. The sewing cuff must retain the sutures, resist degradation, and promote a non-thrombogenic surface.

2.2 *NiTi Core*

The NiTi core gives the SMAC ring its structure and mechanical stiffness. The ring stiffness is dependent on the NiTi material phases: martensitic (the low temperature compliant phase) and austenitic (the high temperature stiffer phase). When heated above a critical temperature (the austenitic start or A_s temperature), NiTi undergoes an internal phase transformation in which the material changes from

a compliant martensitic phase to a rigid austenitic phase (Es-Souni et al., 2005). This phase transition temperature is a function of material composition and heat treatment processes during manufacturing.

For this application, the austenitic shape of the NiTi core is set to conform to the shape of the mitral annulus during the fabrication process. At 24°C or lower, the proposed ring is in the martensitic phase, and can be readily deformed. When heated to 37°C, the NiTi core undergoes a reverse transformation to the austenitic phase; any deformation is fully recovered and the "remembered" shape is restored (Es-Souni et al., 2005). The SMAC ring, in its austenitic phase, is a full ring with unconnected ends. In its martensitic phase, it can be straightened to fit through an 8 mm trocar. Figure 2.1 illustrates the different configurations of the ring as it undergoes the phase transformation from martensite at 24°C to austenite at 37°C.



(a) (b) (c) (d)

Figure 2.1 (a) Ring at 24°C (martensitic phase) is easily straightened; (b-c) changes in shape during heating; (d) ring at 37°C (austenitic phase) in final shape

To determine the requisite mechanical properties of the NiTi core, physical testing was performed on the Physio ring using an EnduraTec (Bose Corporation,

Eden Prairie, MN) material testing machine. These experimental results were used in conjunction with a finite element analysis (FEA) model, Figure 2.2, to facilitate the design process. The FEA model was developed using ANSYS™ Release 9 software (Canonsburg, PA) using 5994 solid92 elements. By simulating compression of the FEA model for a range of elastic moduli (80-120 GPa), it was determined that a Young's modulus of 94.8 GPa best matched the Physio ring's experimental data, Figure 2.3. The posterior portion of the ring exhibited the most displacement, while the anterior remained virtually stationary, which is consistent with published observations (Raffoul et al., 1998).

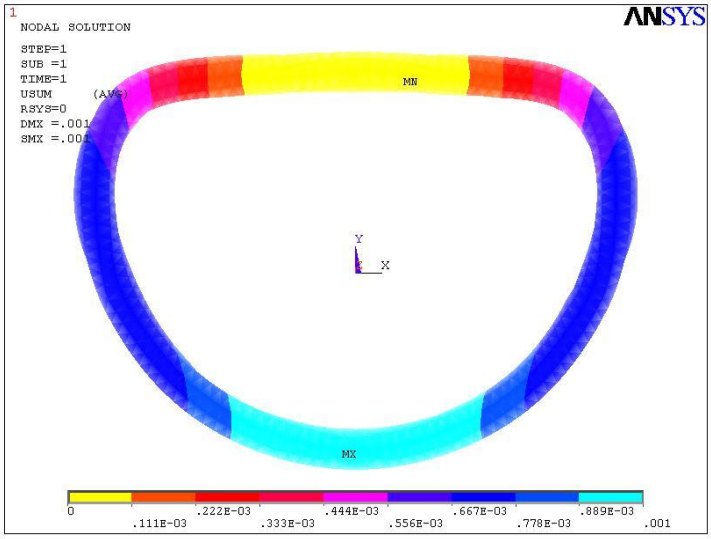


Figure 2.2 ANSYS nodal output model of a Physio ring - response to a 2.0 mm applied displacement

2.2.2 Comparison of Core Materials

A comparison of published data related to the Physio and SJM® rings was completed. The modulus of elasticity, tensile strength, and ultimate tensile strength were compared, Table 2.1. The Physio core is Elgiloy®, or Phynox, which is a Cr-Co-Mo-Ni alloy (Edwards Lifesciences LLC, 2005b), while the SJM® ring has a solid core of UHMWPE (Food and Drug Administration, 2002) . The material properties of

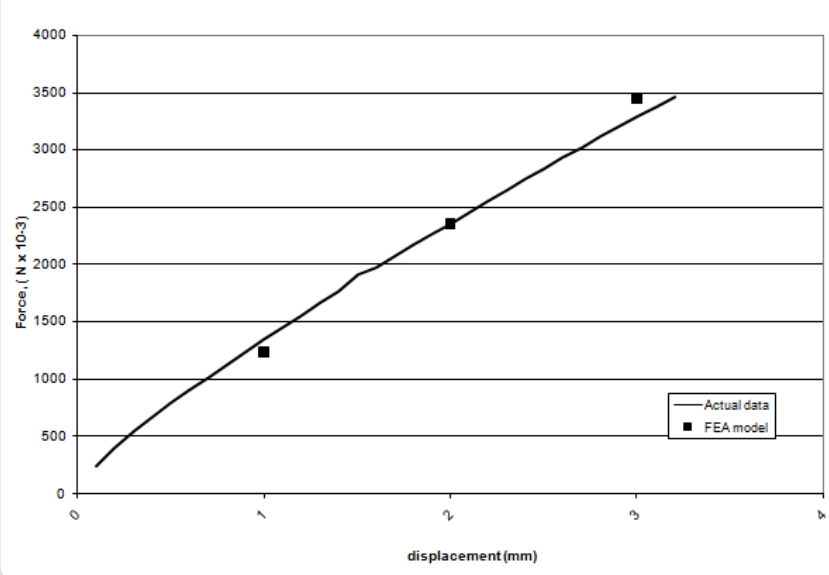


Figure 2.3 Simulated and experimental force versus displacement data for the ANSYS model and actual Physio ring.

the SMAC ring's NiTi core are closer to the lower limit of the Elgiloy® material than the UHMWPE. NiTi's modulus of elasticity in its martensitic state is 63% lower than in its austenitic state. Therefore the NiTi core should be flexible upon deployment.

Upon transformation to the austenite phase there is an increase in the stiffness in order to provide sufficient support for the mitral annulus.

Table 2.1 Comparison of annuloplasty core materials

Property	UHMWPE	Elgiloy® (Phynox)	NiTi
Composition	Polyethylene	Cr 19-21.0% Co 39-41% Fe 16.0% Mn 1.5-2.5% Mo 6-8% Ni 14-16%	Ni 55% Ti 45%
Density (g/cm^3)	.93	8.30	6.45
Ultimate Tensile strength (MPa)	40	970-1940	754-960
Tensile strength, yield (MPa)	26-33	480-1650	100 (M) 560 (A)
Modulus of Elasticity (GPa)	.689	177-194	28 (M) 75 (A)
Comments		Range 20% cold reduction to 40% cold reduction plus heat treatment	

2.2.3 Fabrication Process

Based on the aforementioned design requirements, a 0.51mm diameter NiTi wire in the cold-worked state (55.6 wt% Ni, A_f = 39°C) was obtained from Fort Wayne Metals (NiTi #8, Fort Wayne Metals, Fort Wayne, IN). The exact material composition as specified by the supplier is shown below in Table 2.2.

Table 2.2 Composition of NiTi as supplied.

Chemical	Composition (wt %)
Ni	55.59
C	0.38
Cr	0.01
Fe	0.05
Cu	0.01
Co	0.05
H	0.005
O	0.021
Nb	0.025
All others	0.330
Ti	balance

2.2.4 Shape Setting

The NiTi core required shape setting to conform to the non-planar saddle shape of the mitral annulus. Shape setting is a heat treatment process done using an initial heating to a temperature between 600°C and 900°C, following by a lower temperature annealing process (Ramaiah, Saikrishna, & Bhaumik, 2005; Pelton, Russell, & DiCello, 2003). Generally, long heat treatment times at higher temperatures result in a more exact shape with less springback, and shorter treatment times at lower temperatures result in material closer to the cold-worked material with more shape springback (Pelton et al., 2003).

A brass mandrel, Figure 2.4, was designed and fabricated for shape setting the NiTi wire cores. The mandrel featured a three-dimensional, saddle-shaped groove (32 mm inter-trigone distance) to conform to the natural shape of the mitral annulus. The NiTi wire was wrapped tightly into the groove and secured in place using screws during heat treatment.

Stainless steel pin and plate fixtures were also designed and fabricated to produce 26 mm, 28 mm and 30 mm rings (inter-trigone distance) for use with smaller explanted porcine hearts, Figure 2.5. To obtain the three-dimensional shape, stainless steel washers were used to guide the wire in the z-plane.

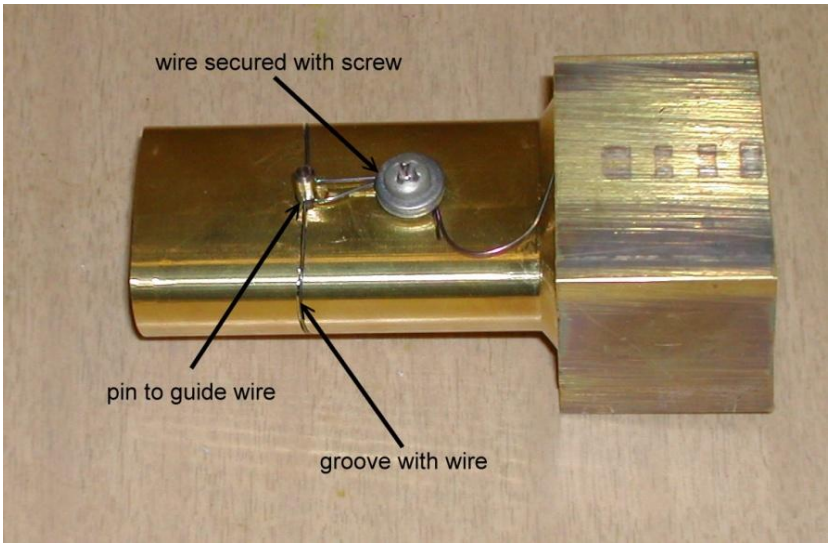


Figure 2.4 Mandrel used for shape setting wire core into three-dimensional saddle shape.

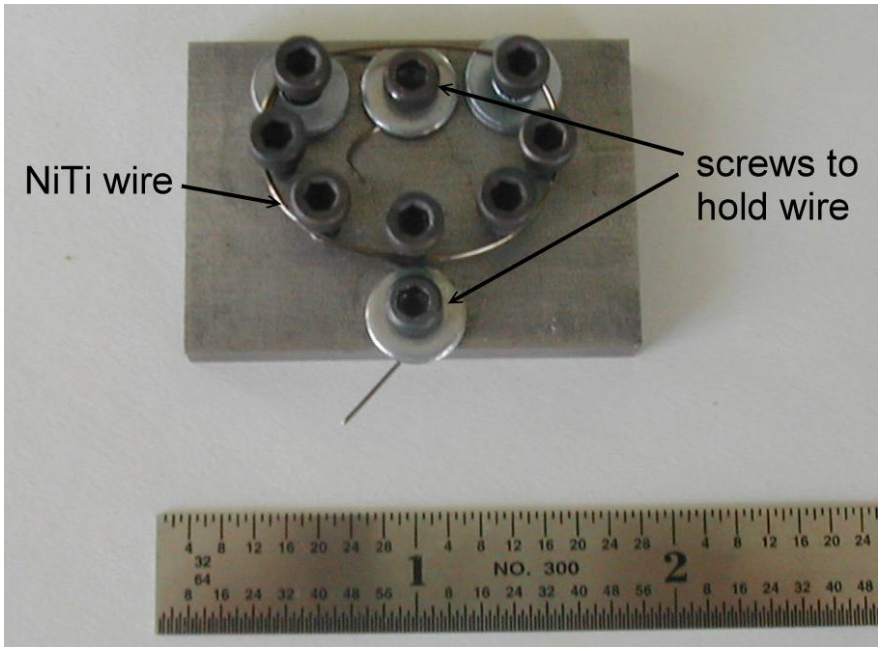


Figure 2.5 Stainless steel pin and plate fixture used to shape set wire core, three fixtures were fabricated one for each ring size: 26 mm, 28mm, and 30 mm.

2.2.5 Adjusting A_f Temperature

The heat treatment process used for shape setting also affects the material's A_f temperature. Between 500°C and 800°C, a precipitation sequence of $Ni_{14}T_{11} \rightarrow N_3Ti_2 \rightarrow Ni_3Ti$ is observed, which increases the A_f temperature (Nishida, Wayman, & Honma, 1986). Nishida et al. (1986) developed time-temperature transformation diagrams that show a maximum increase in A_f temperature at about 450°C(Nishida et al., 1986). However, slight variations in time, temperature and material composition can all greatly affect the A_f temperature (Pelton et al., 2003). Yeung, et al. (2004) examined various cooling methods (air cooling, water quenching and

furnace cooling) and found that the cooling rate also affected the phase transformation temperature (Yeung, Cheung, Lu, & Chung, 2004). Wang, et al. (2004) showed that the A_f temperature could be decreased from 65°C to 39°C when annealed at 600°C and then air cooled (Wang et al., 2004).

To obtain an A_f of 37°C, a design of experiments was conducted that varied the temperature, time and annealing method. Annealing at 600°C for 30 minutes followed by furnace cooling was found to produce the desired A_f of 37°C. Confirmation of A_f temperature was done by compressing the ring in the anterior-posterior direction using a universal testing machine (Applied Test Systems, Inc., Butler, PA) in a temperature-controlled water bath. The anterior portion of the ring was secured using custom fixtures while the posterior portion was compressed 4 mm at a rate of 1 mm/min by a 6.35 mm square mandrel, (Figure 2.6). The temperature of the water bath was controlled using a temperature controller (Athena Controls Inc., Plymouth Meeting, PA) with a stainless steel heating element and a thermocouple. The bath temperature was increased incrementally after each compression cycle. The temperature where the force versus displacement no longer increased was determined to be the A_f temperature, Figure 2.7.

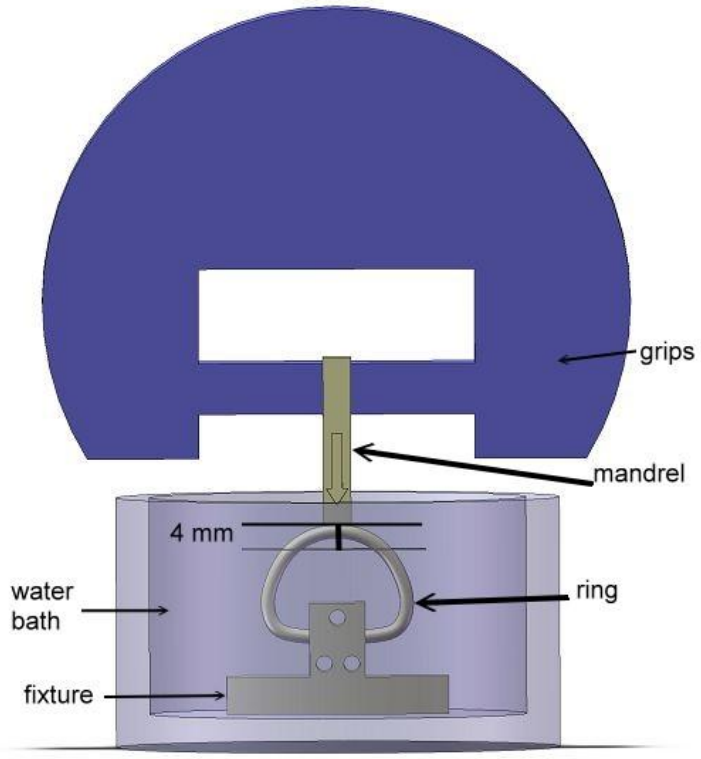


Figure 2.6 Position of ring for A_f confirmation, ring was compressed 4 mm in the anteroposterior direction with a square mandrel on a universal testing machine.

At a displacement of 3 mm, the SMAC ring exhibited an increase in load carrying capacity of 54% when the temperature was increased from 22°C to 37°C. This indicated that wire core should be able to meet the flexibility requirements.

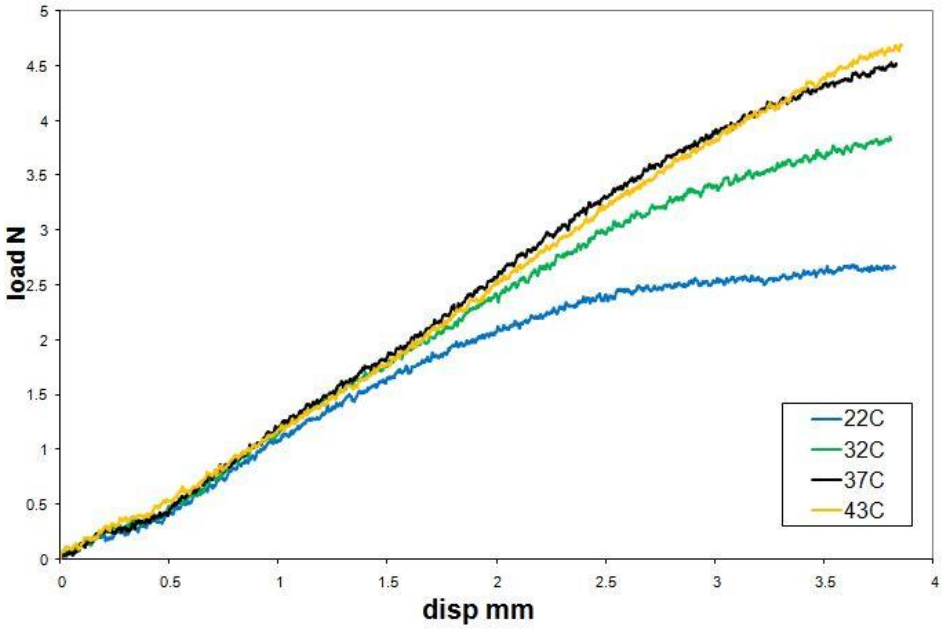


Figure 2.7 A_f temperature confirmation, displacement of 4 mm at increasing temperature, after 37°C the required force stabilizes, corresponding to the A_f temperature.

2.2.6 Fatigue Properties

Understanding of the forces on the ring and the material fatigue properties is necessary to ensure long term success and safety of the annuloplasty ring. The mitral valve is saddle shaped, with the horn of the saddle at the aortic root; during the cardiac cycle the valve undergoes a significant change in shape. Kaplan et al. (2000) studied nine patients by rotational transesophageal imaging. Results showed that there was an inward movement of the posterior annulus toward the anterior aortic root of the annulus of approximately 3 mm which decreases the mitral orifice during aortic filling (mid-systole) (Kaplan et al., 2000). Another study by Dagum et

al. (2001) sutured eight radiopaque markers around the mitral valve annulus of sixteen sheep. (Dagum et al., 2001). During systole, the mitral annulus flexed in the anterior-posterior direction 2.3 ± 4 mm with the maximum at late diastole and a minimum at mid-systole (Dagum et al., 2001).

The dynamic movement of the annulus places a cyclical force on the annuloplasty ring (Arita, Kasegawa & Umezu, 2004). Arita et al. (2004) used an *in vitro* static evaluation test system to quantify these forces on two types of planar rings, one flexible and one rigid. The test system consisted of silicone sheets with weights attached to change the orifice area to mimic the cardiac cycle; annulus load was measured at eight points around the ring (Arita et al., 2004). The maximum resulting force on a 35 mm flexible ring was found to be 1.96 N, and the maximum force on a 36 mm rigid ring was slightly higher at 2.21 N (Arita et al., 2004). The load found in both rings was greater in the posterior region than in the anterior region (Arita et al., 2004). Although these forces do not seem large, there have been several reported fractures of the CG Future® band (Medtronic, Inc., Minneapolis, MN) (U.S. Food and Drug Administration Center for Device and Radiological Health, 2009). The CG band has a core of MP35N, a nickel-cobalt-chromium-molybdenum alloy. Hartrump et al. (2006) reported a case in which a 56 year old patient had undergone mitral repair with a 36 mm partial band. Ten months later he was readmitted with symptoms of congestive heart failure and severe mitral regurgitation (Hartrumpf, Stock, Kuehnel, & Albes, 2006). Upon re-operation, it was

found that the metal core of the band was fractured near the posteromedial commissure and the wire had perforated the silicone sheathing and the cloth sewing cuff causing a tear at the base of the A3 anterior leaflet (Hartrumpf et al., 2006). The band was still sutured to the annulus with eleven sutures, none of which were torn or loose and the band itself was in no other way defective other than the fractured metal core (Hartrumpf et al., 2006). The authors speculated that the fracture was due to material fatigue caused by the inherit deformation of the ring during the cardiac cycle citing the location of the fracture which occurred at a flex point (Hartrumpf et al., 2006). A review of the FDA Center for Devices and Radiological Health MAUDE (Manufacturer and User Facility Device Experience) database indicated that this was not the only incident of fracture of the CG Future® Band. There were four incidents reported in 2005 and two in both 2006 and 2007, see Table 2.3 below. The MAUDE data is a voluntary reporting system of adverse incidents involving medical devices; therefore all incidents are not required to be reported (U.S. Food and Drug Administration Center for Device and Radiological Health, 2009).

Table 2.3 CG Future® band adverse incidents reported to FDA in MAUDE in which there was a fracture of the core, from 2005-2008.

Event date	Patient Problem	Time from initial implant (months)	Action	Manufacturer Narrative Summary
1/20/2005	not stated	4	replace with a valve	Fabric in area of fracture showed no signs of damage. Wire fracture initiated at a subsurface inclusion in the wire. Broken at the center or mid-point of the product as noted by x-ray. Met all specs when released to distribution
2/23/2005	removed band	11	not stated	Wire fracture along left side of device when viewing from the mitral valve flow side, at approx. 8-9 o'clock position, fracture is along the inner curvature.
10/10/2005	mitral insufficiency LV dilation and heart failure	13	replaced	Device met specs when shipped. Radiography showed break in the stiffener wire of the band. Fractured wire did not penetrate silicone and cloth layers.
10/27/2005	mitral insufficiency 3 yrs after initial implant	41	replaced	Device met specs when shipped. Radiography showed break in the stiffener wire of the band. Fractured wire did not penetrate silicone and cloth layers.
6/19/2006	dehiscence	34	replaced with valve	Band was fractured where the band dehisced from the annulus.
9/29/2006	fracture noted during angiogram	30	replaced with valve	Break in wire approx 1.5 cm from one end. Broken end protruding through the cloth cover. Sept 2004 corrective action was taken to improve the stiffness of the wire and this band was manufactured prior to this correction action
1/26/2007	regurgitation of 4+	25	not stated	Product not yet returned, surgeon notes that band was fractured during explantation of the band.
2/12/2007	severe mitral regurgitation	20	replaced with valve	Band was fractured at the center posterior position, product met spec when released for distribution, exact cause of fracture is underway.

Factors such as the shape and flexibility of the ring, suture placement, amount of remodeling and mitral valve anatomy all contribute to the forces acting on the ring (Kaplan et al., 2000). The ring core must be able to maintain support of the mitral annulus over the patient's lifetime.

Although NiTi has been shown to be stable within the body (Es-Souni et al., 2005; S. A. Shabalovskaya, 1996) the ring material properties must maintain sufficient stiffness while being subjected to cyclical loading during the cardiac cycle. Constitutive properties of many metals change with cyclical loading. The support structure of the SMAC ring is the NiTi wire core which is in the austenite state when at body temperature. Deformation of the ring will cause the reversible transformation to stress-induced martensite. McKelvey and Richie (1999) found that at a strain of 6.4%, peak stress decreased with repeated cycles, indicating cyclic softening (McKelvey & Ritchie, 1999). The magnitude was largest between the 1^{st} and 10^{th} cycle, and decreased with further cycling (McKelvey & Ritchie, 1999). When cycled up to 100 cycles; cyclic softening reached a saturation point at the 60^{th} cycle, and the residual plastic strain plateaued at 2.1%. (McKelvey & Ritchie, 1999). When cycled below the plastic yield point the material remained superelastic with reversible strains of approximately five percent (McKelvey & Ritchie, 1999).

Tolomeo et al. (2001) performed cyclical testing on NiTi wire with an A_f 28 ± 2°C in a water bath at 37°C (Tolomeo, Davidson, & Santinoranont, 2001). They

compared the cyclic stress /strain with monotonic stress/strain in fixed amplitude testing (note: did not give wire diameter, cycle frequency, composition of NiTi or any heat treat/processing history). The results showed a reduction in stress with increasing strain amplitude which corresponds to an increase in the stress induced martensite (Tolomeo et al., 2001). At lower strain amplitude, approximately 1% strain, prior to the plateau region, monotonic and cyclic stress levels were equivalent (Tolomeo et al., 2001). In the plateau region, the cyclical stress was less than the monotonic stress for a given strain (Tolomeo et al., 2001). The difference in the stress between the cyclic and monotonic testing was minimal at strain values less than 2%. The difference in the stress gradually increased and was the greatest at an approximate 7% strain (Tolomeo et al., 2001). Researchers concluded that this cyclic softening during the transition of the austenitic phase to stress-induced martensite is attributed to the reorientation of the grain and dislocation movement, and higher cyclic stress will increase cyclic softening.

Tolomeo et al. (2001) also investigated the fatigue properties of superelastic stents at eight different prestrain values ranging from 0.5% to 6%. Testing concluded that at half amplitude alternating strain of less than 0.6%, cycles to failure of NiTi stents exceeds one million cycles; up to a 6% prestrain (Tolomeo et al., 2001). Results showed that the fatigue limited was not correlated with the prestrain, and the endurance limited remained relatively constant across the prestrain range. A drawback of this research was that material composition and processing history

was not specified. Mechanical properties of NiTi such as transition temperature, tensile strength, yield strength, ductility and others are dependent on material composition (Pelton et al., 2003).

Fatigue growth rates of specimens with different compositions of NiTi were studied by Dauskardt et al. (1989) at room temperature. Stable martensite and austenite have similar higher fatigue thresholds, while stress-induced martensite had a lower fatigue threshold and higher crack growth rate (Dauskardt, Duerig, & Ritchie, 1989). Results showed that fatigue thresholds are dependent on the composition as well as transition temperature and therefore should be considered when evaluating NiTi devices (Dauskardt et al., 1989).

Tobushi et al. (1998) investigated the influence of strain rate on the superelastic properties of NiTi and found that at strain rates above 10%/min the martensite transformation stress and temperature of the material increased, while at strain rates below 2%/min the superelastic properties do not depend on the strain rate and there is no increase in material temperature. During loading, while stress/strain was in the plateau region, the interface between the austenite phase and the martensite phase moved as a function of the stress, the stress-induced transformation to the martensite phase progressed until the material was entirely martensite (Tobushi, Shimeno, & Hackisuka, 1998). The researchers concluded that at a lower strain rate, there was time for the interface to move and stress area to

relax (Tobushi et al., 1998). At a higher strain rate, the interface moved quickly and there was little time to relax the stress, internal friction built, and as a result temperature increased (Tobushi et al., 1998). Although high cycle fatigue testing is currently used for many device designs, this may not accurately represent NiTi devices (Tobushi et al., 1998).

2.3 *Silicone Sheathing*

The cross sectional diameters of the commercial Physio and SJM® rings are approximately 3.0 mm. Two medical grades of silicon tubing approximating this dimension were evaluated. The larger tubing had an outside diameter of 4.36 mm and a wall thickness of 2.38 mm. The smaller tubing had an outside diameter of 2.38 mm and a wall thickness of 0.79 mm. Additionally, a custom silicone sheath was fabricated from MoldMax 30™ (Smooth On, Easton, PA) with an outside diameter of 2.54 mm. Although the custom mold was in the final saddle shape around the wire, it was determined that the molded silicone decreased the overall flexibility of the ring. The smaller surgical tubing (2.38 mm OD) had less effect on the ring's compliance, and met FDA and ISO 10993 biocompatibility standards. For this reason it was chosen for subsequent prototype evaluations.

2.4 *Sewing Cuff*

The sewing cuff is intended to be in direct contact with the mitral valve annulus; therefore, it must be biocompatible and be able to retain the sutures. Loose material or stray threads could lead to a thromboembolism; therefore it is critical that the sewing cuff fit snugly around the silicone sheathing. Polyester materials are biocompatible and durable and have been used for heart valve sewing rings, vascular grafts and endovascular stent grafts (Weinberg & King, 2004). The sewing cuff on the Physio ring was determined to be a coarse, single knit polyester fabric, while the SJM® sewing cuff was made from weft knit polyester, Figure 2.8.

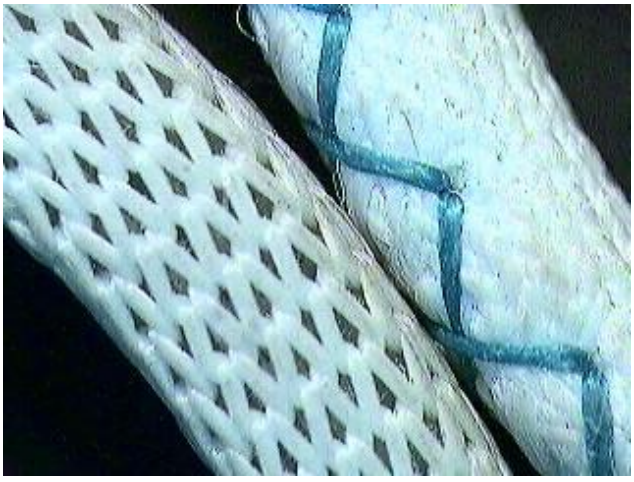
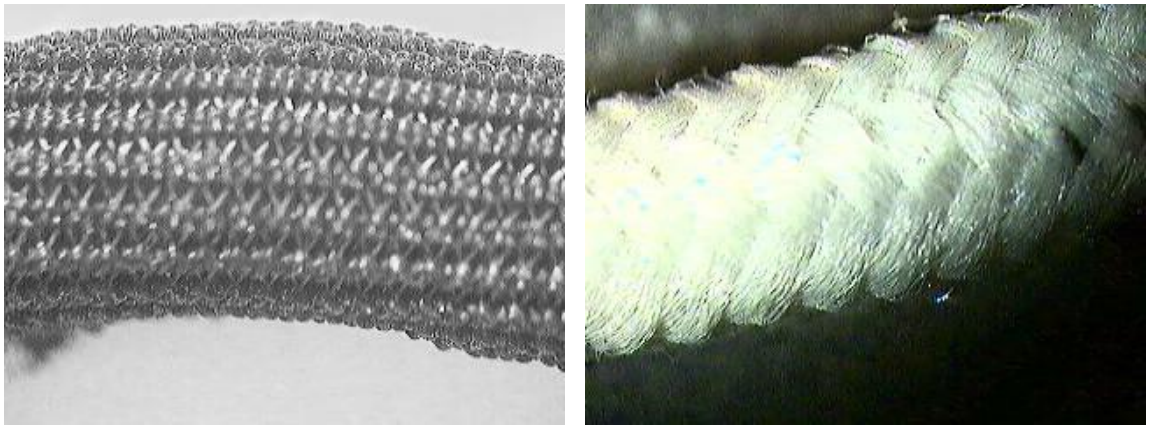


Figure 2.8 Magnification (2x) of the Physio ring on the left and the SJM® ring on the right showing variations in the polyester knit of the Physio versus the weft knit of the SJM® ring.

Two types of sewing cuff material were investigated for the SMAC ring. One was a polyamide 6 knit fabric and the other a circular braided polyester (Figure 2.9). The knit fabric fit more securely on the silicone tubing and therefore was selected.



(a) (b)

Figure 2.9 Magnification (2x) of SMAC sewing cuff materials. (a) nylon knit material, (a) circular braided polyester

2.5 *Preliminary Evaluations*

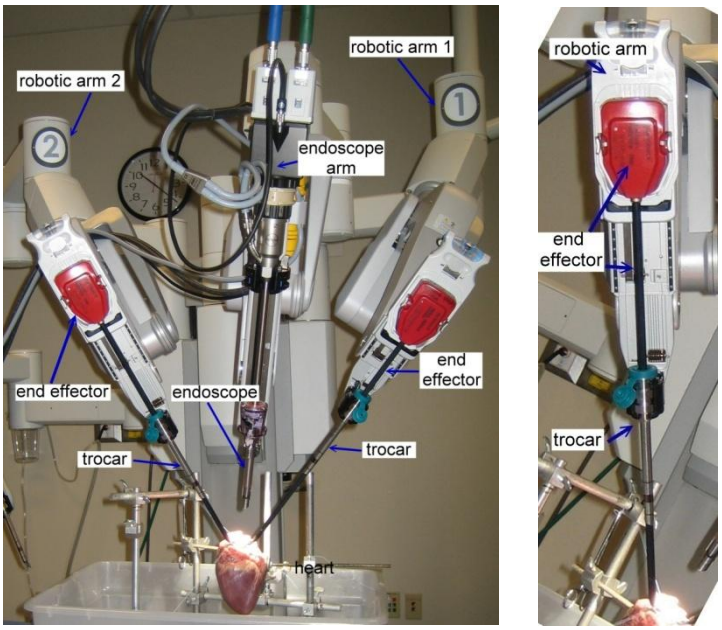
Preliminary evaluations included deployment of the SMAC ring with an 8 mm trocar and an initial surgical evaluation conducted by a cardiothoracic surgeon trained in robotic mitral valve repairs.

2.5.1 Trocar Insertion

A trocar is a portal that allows the insertion of various end effectors which attach to the robotic arms to be inserted into the body. They are inserted into the body through a stab incision; the various end effectors can then be interchanged

through the trocar. The trocars can also be used to insert suture and the flexible ring.

The standard minimally invasive mitral valve repair procedure utilizes two 8 mm trocars for placement of the robotic instruments, and a 4-6 cm working access port in the 4th intercostal space (Casselman et al., 2003). The trend is toward a



(a) (b)

Figure 2.10 (a) Set up of da Vinci Surgical Robot with two robot arms with 8 mm trocars, and one arm with the endoscope. (b) End effector attached to robotic arm, passes through the 8 mm trocar.

totally endoscopic surgery without a working port, reducing incision size to only the stab incisions for the trocars. Mehmanesh and colleagues (2002) recently reported

a successful totally endoscopic mitral valve repair using one 12 mm port for the endoscope, and three 10 mm ports – two for robotic instruments and one for passing sutures and a flexible ring (Mehmanesh, Henze, & Lange, 2002).

The SMAC ring was easily straightened and successfully deployed through an 8 mm trocar Figure 2.11. The semi-rigid Physio could not be deformed, and therefore could not be deployed through the 8 mm trocar, as shown in Figure 2.12

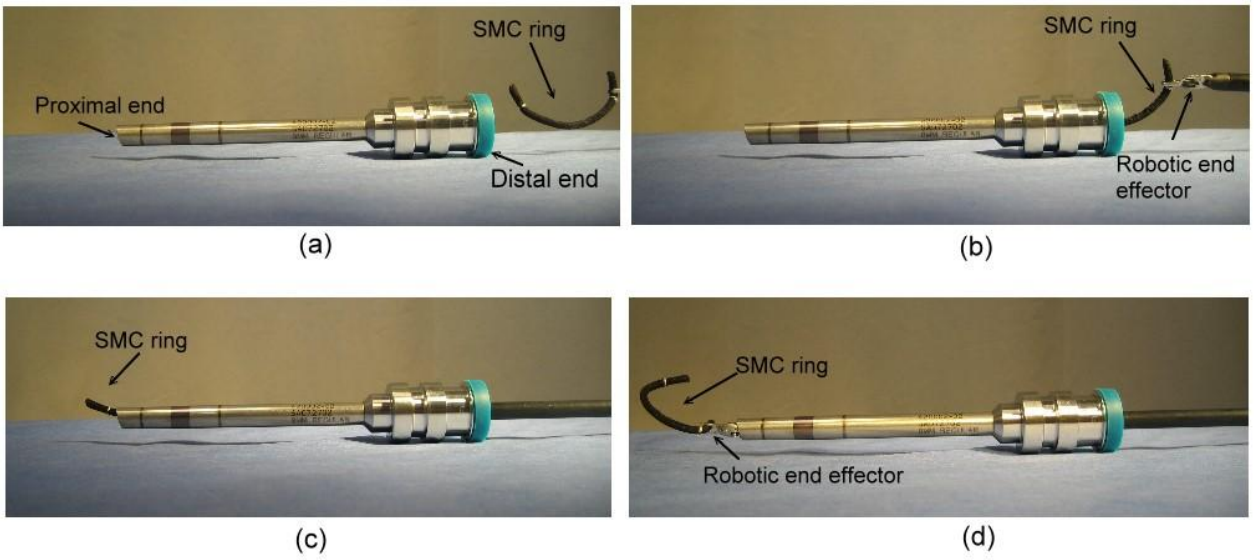


Figure 2.11 (a – d) SMAC ring straightened and deployed through 8 mm trocar with the robotic end effector.



(a)



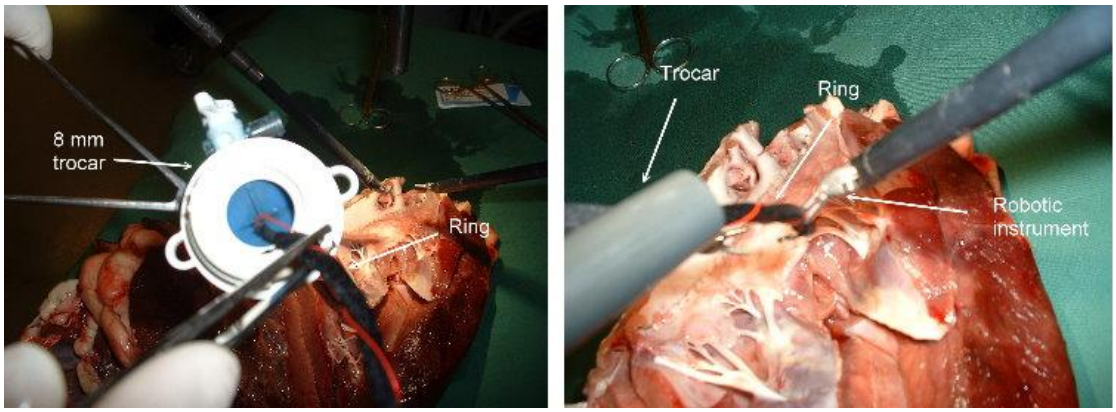
(b)

Figure 2.12 (a) and (b) Semi -rigid Physio ring cannot be inserted through the 8 mm trocar.

2.5.2 Surgical Evaluations

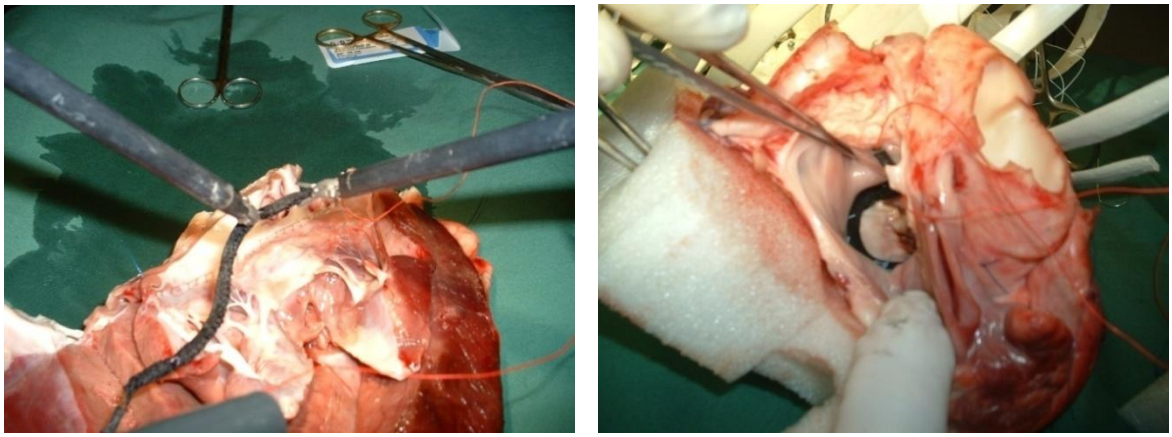
Initial surgical evaluations were conducted by Dr. Gil Bolotin, a robotically trained cardiothoracic surgeon, at the Academic Hospital Maastricht, Netherlands. The ring in its flexible martensitic state was successfully introduced through an 8 mm trocar into an explanted bovine heart using the da Vinci Surgical System (Intuitive Surgical Inc., Sunnyvale, CA), Figure 2.13 and Figure 2.14. The ring was activated by Joule heating; the NiTi core was transformed into its stiffer austenitic state and

the ring obtained the desired shape. After positive surgical feedback, additional quantitative evaluations were planned.



(a) (b)

Figure 2.13 Surgical evaluations using the da Vinci Surgical System: (a) SMAC ring being deployed through an 8 mm trocar, (b) ring being manipulated and secured using robotic instruments.



(a) (b)

Figure 2.14 (a) Robotic tools manipulated ring easily before activation. (b) SMAC ring sutured into explanted bovine heart and activated through Joule heating

Chapter 3 Methods and Materials

To determine the efficacy of this novel annuloplasty design, five *ex vivo* studies were performed. Mechanical testing compared the compressive force versus displacement of the SMAC ring to the Physio and SJM® rings. To evaluate the effectiveness of each ring in correcting mitral valve regurgitation (MVR), static pressure tests were conducted by a cardiothoracic surgeon using explanted porcine hearts. Dynamic flow comparisons to the Physio ring were performed on a left heart pulse duplication system. Cyclic fatigue tests were performed to ensure that the SMAC ring's NiTi core would resist cyclic softening or cracking. Finally, qualitative robotic manipulation comparisons between a SMAC ring and a semi-rigid Physio ring were completed. This chapter details the testing methods and materials.

3.1 *Mechanical Testing*

Mechanical properties of the activated NiTi core ring were compared to commercially available semi-rigid rings. The semi-rigid rings targeted were the Carpentier Edwards Physio and the SJM® Séguin. Compression tests were conducted using an ATS universal testing machine (Applied Test Systems, Inc. Butler, PA), Figure 3.1. Mechanical testing of the ring was conducted with the NiTi in its austenite state (37°C), which represents the final state for the implanted ring.

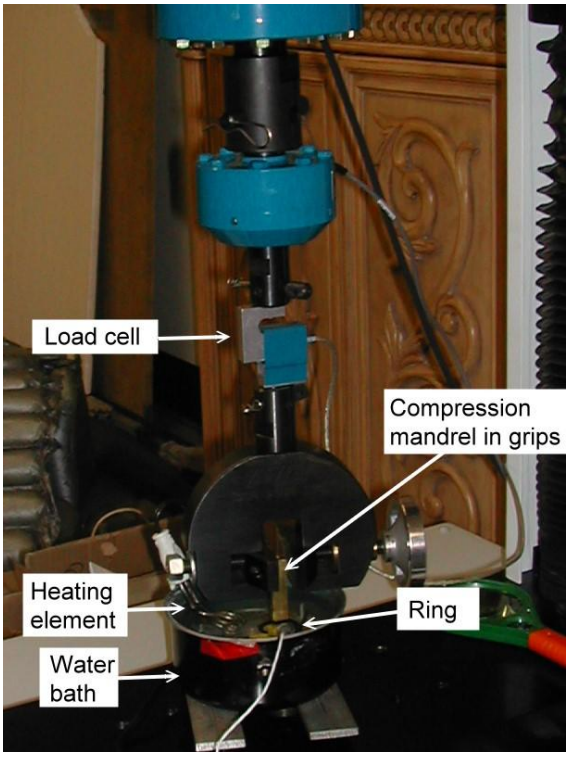


Figure 3.1 Photograph of the universal testing machine used for temperature-controlled experiments

Additional tests were conducted in the martensite state (24°C) to illustrate the SMAC ring's compliance during deployment. All rings were compressed 4 mm in the anterior-posterior orientation at a 2.5 mm/min loading rate. Rings were secured in a customized fixture on the anterior side in a water bath in the same manner as A_f temperature testing described previously. The rings were compressed with a 6.4 mm square mandrel, Figure 3.2.

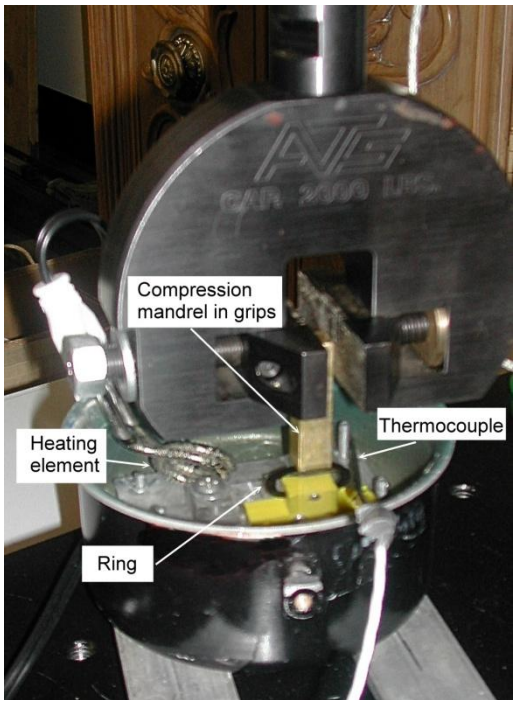
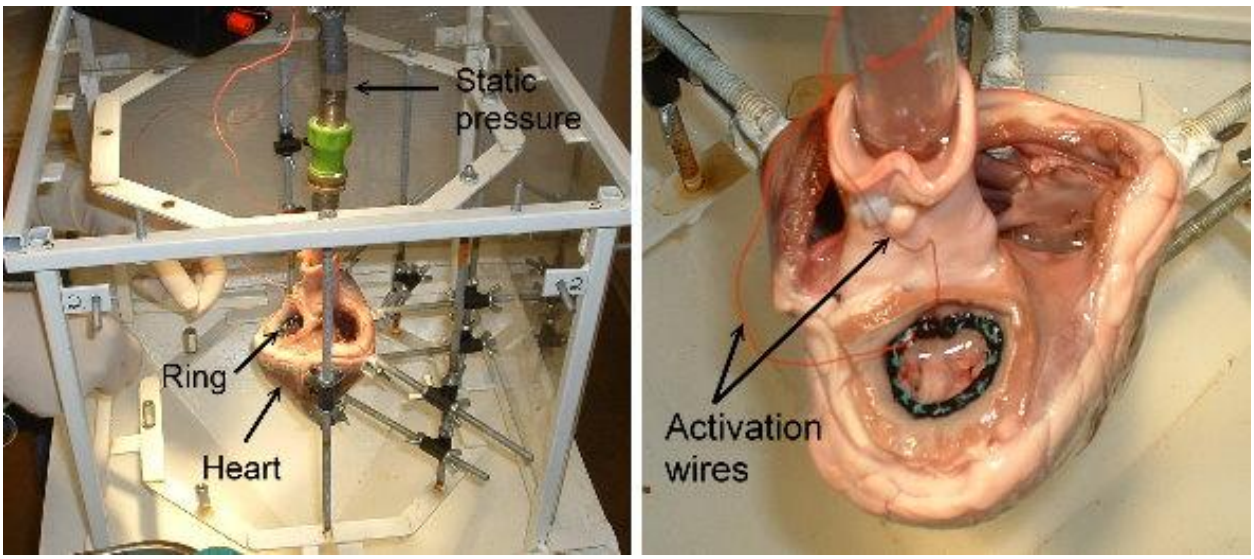


Figure 3.2 Photograph of the temperature-controlled water bath. Ring is compressed in anterior-posterior direction by the mandrel

3.2 *Static Pressure Evaluations*

To evaluate the efficacy of the SMAC ring, static pressure tests were performed by Dr. Richard Cook, a cardiothoracic surgeon, at Vancouver General Hospital, Vancouver BC. An explanted porcine heart, from a 70-100 kg swine, was mounted in a fixture and the left atrium was removed to access the mitral valve, Figure 3.3. Mitral valve regurgitation (MVR) was induced by cutting several of the chordae tendinae along the middle scallop of the posterior leaflet, thereby creating severe mitral regurgitation with a flail “P2” segment (Carpentier, 1976) of the

posterior leaflet. Back-pressurizing the valve to 108 mm Hg was accomplished using a static column of saline solution. Mitral regurgitation was assessed by collecting and measuring the saline solution that flowed back through the valve. The SMAC ring was sutured into place and then activated by Joule heating. Mitral regurgitation was again quantified.



(a) (b)

Figure 3.3 (a) Explanted porcine heart with left atrium removed, secured in fixture for static pressure testing. Static column of saline provides back pressure on mitral valve. (b) Ring sutured into porcine heart and active by Joule heating, wires connected to a power supply.

3.3 *Dynamic Flow Testing*

To evaluate the SMAC ring in a more physiologically realistic environment, dynamic flow testing was completed using a left ventricular pulse duplication system (Richards, Cook, Bolotin, & Buckner, 2009). This system dynamically pressurizes explanted porcine hearts, repeatedly subjecting the mitral valve to pressure waveforms and flow rates similar to those found *in vivo,* Figure 3.4. The system allows for control of numerous parameters, including stroke rate (heart rate), systolic fraction, and stroke volume. By measuring changes in cardiac output and left heart pressures, mitral regurgitation in this system can be quantified.

A randomized study using five Physio rings and five SMAC rings was conducted using a stroke rate of 60 strokes per minute and a systolic fraction of 35%. Each ring was surgically sutured in a separate freshly explanted heart. A 0.9% saline solution heated to 40°C was pumped through the system. The stroke volume was adjusted for each heart depending on size and tissue compliance and ranged from 35 ml/stroke to 40 ml/stroke. The stroke volume was kept constant throughout each experiment to ensure constant fluid input. Because of the unique anatomy and tissue compliance of each heart, a baseline aortic output measurement was initially taken. For each baseline measurement, aortic outflow resistance was increased until peak ventricular pressure reached 120 mmHg; the heart was then dynamically pressurized for 1 minute while the aortic output was collected and measured. The

left ventricle pressure was then increased to 150 mmHg, simulating a stressed heart, and output again was measured.

An atriotomy was performed to expose the mitral valve. Valve failure was induced by stretching the mitral annulus in the anterior-posterior and transverse directions until a significant increase in the anterior-posterior distance occurred without decreasing the transverse length to simulate annular dilation. Additionally, chordae tendineae connecting the P2 leaflet (Carpentier, 1976) to the papillary muscles were severed to simulate chordal rupture. The valve was subjected to 35

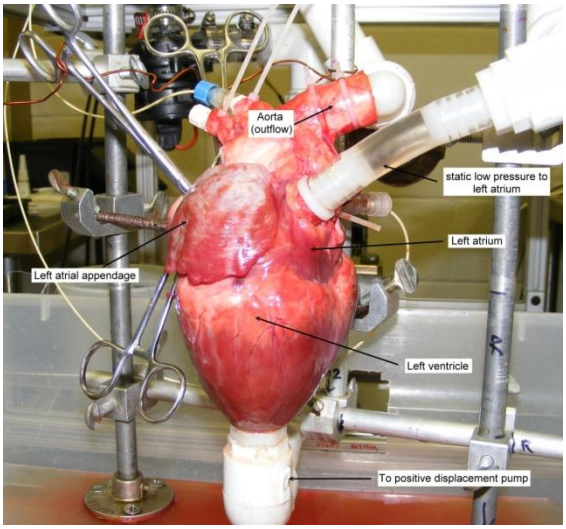
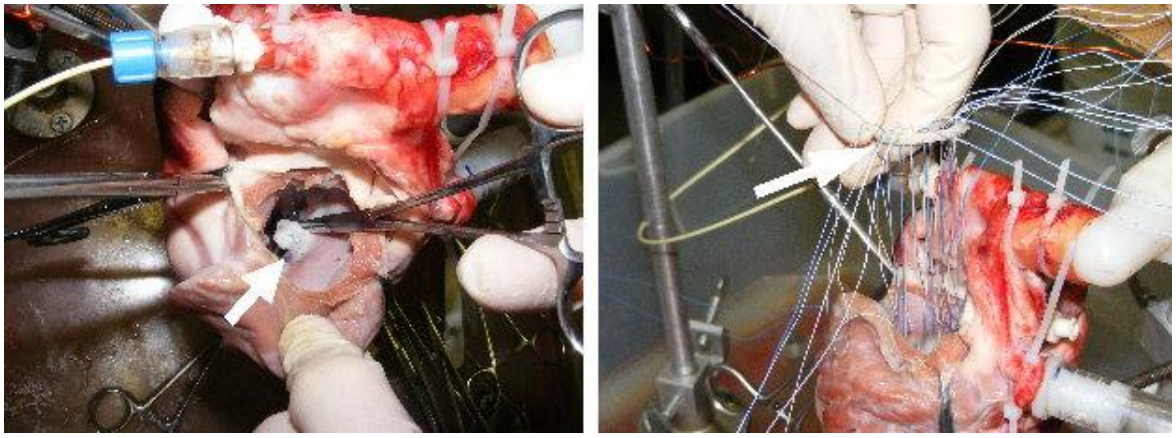


Figure 3.4 Explanted porcine heart connected to the left pulse duplication system. (Richards et al., 2009)

mm Hg static backpressure to ensure adequate mitral valve failure. The incision from the atriotomy was closed with cyanoacrylate adhesive and suture. Output

measurements were repeated at both 120 and 150 mmHg peak left ventricular pressure for one minute.

In order to perform the repair, the atriotomy was reopened to expose the mitral valve. The valve was repaired with a triangular resection and leaflet reapproximation using a running monofilament suture (4-0 Prolene, Ethicon, Sommerville, NJ), Figure 3.5 (a). All rings were sutured to the annulus using the parachute technique, Figure 3.5 (b).



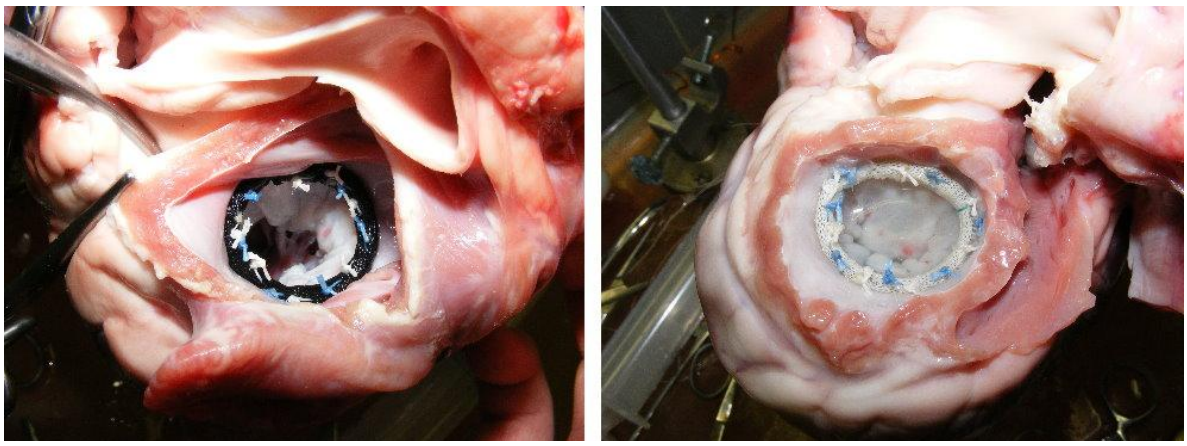
(a) (b)

Figure 3.5 (a) Leaflet repair after triangular resection using running monofilament suture, arrow indicates repair. (b) Physio ring inserted into using parachute technique

The ring size was determined by the physical anatomy of the annulus, which ranged from 26 mm to 31 mm trigone to trigone distance. The rings were secured to the annulus using interrupted horizontal mattress sutures with an average of 12.6

(range 12-14) sutures per ring using 2-0 TI•CRON braided polyester sutures (USS, Norwalk, CT), Figure 3.6.

Static pressure was used to ensure there was no leakage through the valve before closing each atriotomy. The output measurements were again taken at 120 mm Hg and 150 mm Hg peak left ventricular pressure for one minute. Endoscopic images of implanted Physio and SMAC rings are shown in Figure 3.7.



(a) **(b)**

Figure 3.6 Static pressure check before closing atriotomy: (a) SMAC ring, 26 mm (b) Physio ring, 26 mm

3.4 *Fatigue Testing*

An ANSYS simulation on the NiTi wire was utilized to estimate the material strain at the maximum bend radius of the ring (at the commissures). Parameters used in the model are shown in Table 3.1. Although mitral valve displacement has

been shown to be approximately 3 mm (Kaplan et al., 2000;Dagum et al., 2001), a displacement of 4 mm was utilized in order to evaluate an extreme condition. The displacement resulted in computed strains at the maximum bend radius ranging from 0.0225 mm/mm to 0.0065 mm/mm. The strain is within the plateau region of the stress/strain diagram, indicating stress induced martensite is present.

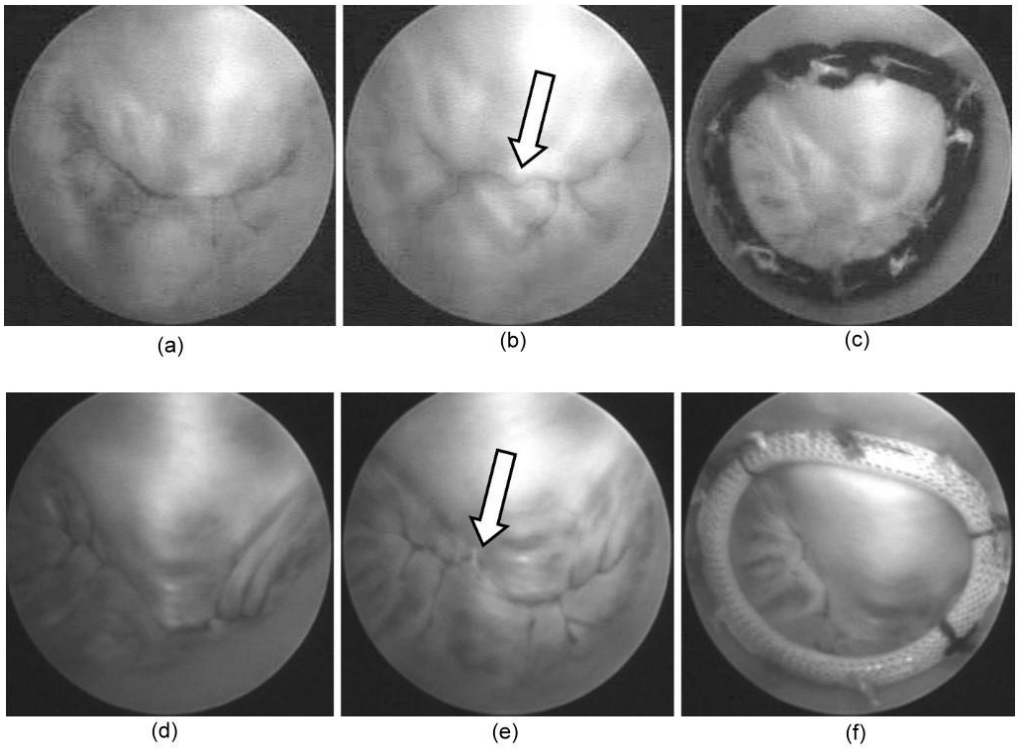


Figure 3.7 Endoscopic pictures during dynamic flow testing. (a) and (d) Normal mitral valve, (b) and (e) Valve after mitral regurgitation has been induced, arrow indicates flail leaflet. (c) Repaired valve with the SMAC ring. (f) Repaired valve with the Physio ring.

Table 3.1 Material Properties of NiTi wire core used for ANSYS model (TiNi Alloy Company)

Material Property	Value
Modulus of Elasticity	75 GPa
Poisson's Ratio	0.30
Density	6.45 g/cc

Cyclical fatigue testing was conducted with the SMAC ring secured in custom aluminum fixtures. The anterior portion of the ring (with open ends) was secured in the fixture with ends fixed to the base. The posterior portion of the ring was secured and the fixture was connected to a 10g load cell (Model MLP-10, Transducer Techniques Inc., Temecula, CA) driven by a linear actuator (LinMot model PS01-37x120, LinMot, Inc., Elkhorn, WI). To simulate annulus movement during the cardiac cycle, the ring was subjected to a sinusoidal displacement amplitude of 4 mm in the anterior-posterior direction. A custom LabVIEW Real-Time 8.2 (National Instruments, Austin, TX) "virtual instrument" was developed to control the actuator and coordinate data acquisition. A sampling rate of 2.0 Hz was used for a total of 1.9 million cycles, which is equivalent to approximately 3.3 weeks *in vivo*. Position and force data for two sinusoidal periods was recorded every one thousand cycles.

During the fatigue test, the ring was held at a constant temperature of 37°C in a water bath of distilled water. Distilled water was chosen based on the fatigue

crack growth research results of McKelvey and Richie (1999) which studied NiTi in air, deionized water and aerated Hank's solution at 37°C using stress-intensity control on servo-electro hydraulic machines at 10Hz. Results showed no significant difference of corrosion fatigue in Hank's solution compared with the air and deionized water (McKelvey & Ritchie, 1999). A commercial temperature controller (Athena Controls Inc., Plymouth Meeting, PA) with a stainless steel heating element and thermocouple positioned near the ring was used to regulate the temperature of the water bath. The fatigue test was terminated at 1.9 million cycles due to an electrical power outage. The power outage also damaged the ring; therefore compression testing was not completed on the ring after fatigue testing.

3.5 *Robotic Manipulation*

Qualitative comparisons of deployment and robotic manipulation were made between a SMAC ring in its flexible martensitic state and a Physio ring. Evaluations were conducted using a da Vinci Surgical System by Dr. Richard Cook, a cardiothoracic surgeon trained in robotic procedures at the Intuitive Surgical Training Center in Sunnyvale, CA. Ease of manipulation with the robotic instruments, visualization of the mitral annulus, tension on the sutures, and deformation of the

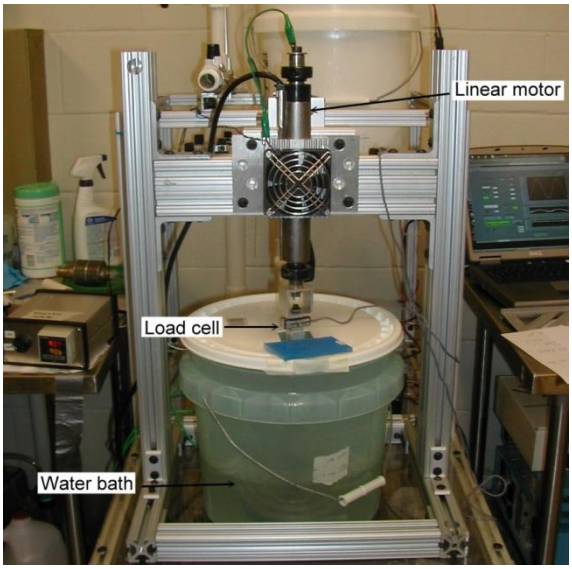


Figure 3.8 Fatigue testing apparatus, ring and fixtures are in water bath

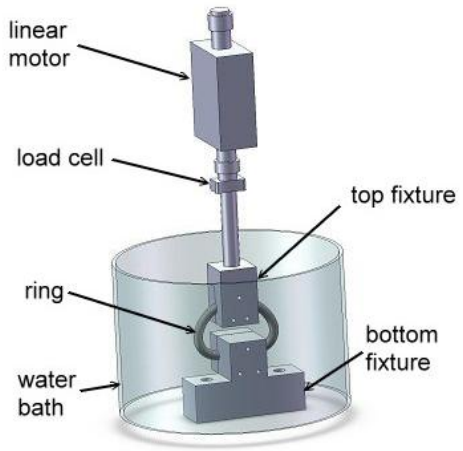


Figure 3.9 Solid model of fatigue testing set up, anterior of ring is held fixed; posterior is displaced 4 mm per cycle at rate of 2 Hz.

surrounding annulus tissue were evaluated. All suturing, ring manipulation and knot tying was done robotically. An explanted porcine heart was placed in a holding fixture and a standard left atriotomy was performed to expose the mitral valve, Figure 3.10.

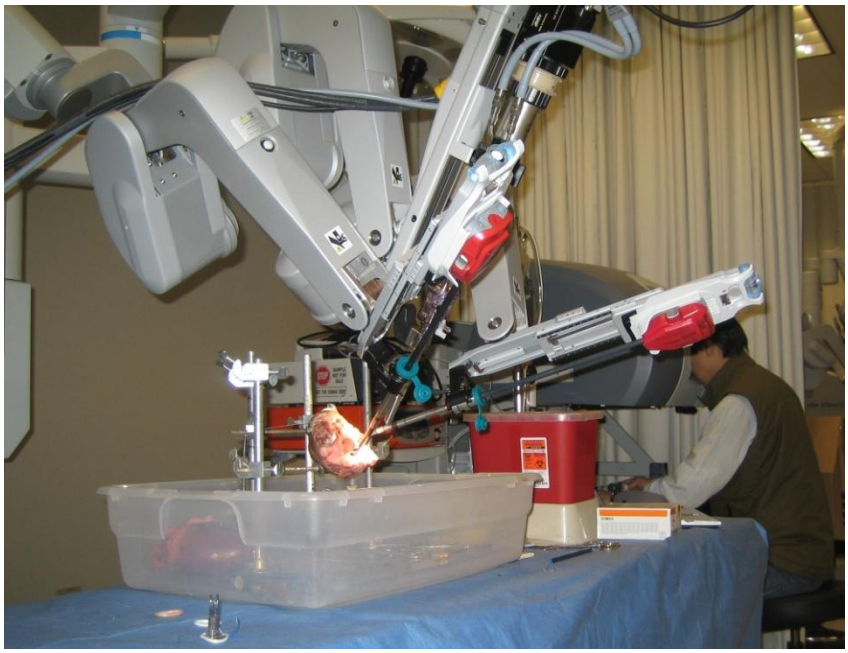


Figure 3.10 Set up for robotic evaluation with porcine heart placed in fixture. The da Vinci Surgical robot with two robot arms and endoscope attached. Surgeon seated at console.

Each ring was sutured to the annulus using individually inserted and knotted sutures without the use of an annuloplasty ring holder to simulate the minimally invasive procedure. Two Physio and two SMAC rings were sutured into four separate hearts. In each trial, the placement of the first suture was varied to

evaluate multiple methods of insertion, Table 3.2. The first trial used a Physio ring with the first suture placed in the left trigone. The following sutures went across the anterior to the left trigone, then along the posterior, continuing around the annulus. A SMAC ring was used for the second trial with the first suture in the right trigone. Sutures continued clockwise around the annulus. The third trial used the same suture method as the second trial however; the third trial used a Physio ring. The fourth and final trial used a SMAC ring that was sutured first on the left trigone, then on the right trigone. The following three sutures were placed along the posterior section securing both ends together with a single suture. The sutures continued on alternating sides, with the final suture in the mid-posterior section. By securing both ends of the SMAC ring initially, the fourth trial represented a worst-case scenario for the SMAC ring.

Table 3.2 Robotic evaluation trials indicating various suture methods

Trial	Ring Type	Size	Location of 1st suture	Direction of subsequent sutures	Total sutures
1	Physio	30 mm	Left trigone	Anterior	13
2	SMAC	28 mm	Right trigone	Posterior	15
3	Physio	26 mm	Right trigone	Posterior	13
4	SMAC	26 mm	Left and right trigone	Anterior	16

Chapter 4 Results

4.1 *Mechanical Testing*

Results from the mechanical testing of the SMAC ring, Physio ring and Séguin ring are shown in Figure 4.1. The mechanical testing indicated that the force versus displacement for the SMAC ring is within 5.0% of the force versus displacement for the commercially available rings. At a displacement of 3mm, which has been shown to be the average displacement of the mitral valve annulus (Dagum et al., 2001; Kaplan et al., 2000), the SMAC ring force is within 4.3% of the Physio ring and within 7.3% of the Séguin ring. In addition, the increase in stiffness from the martensitic phase at 24°C to the austenite phase at 37°C demonstrates the ring's two-phase characteristics. At an anterior-posterior displacement of 3 mm, the activated (austenitic) SMAC ring was 80.5% stiffer than the same ring in its non-activated (martensitic) state. .

4.2 *Static Pressure Testing*

The results from the static pressure trials are shown in Table 4.1. Mitral regurgitation (MR) is the amount of fluid that flows back through the mitral valve when the valve is in the closed position, instead of flowing through the aortic valve.

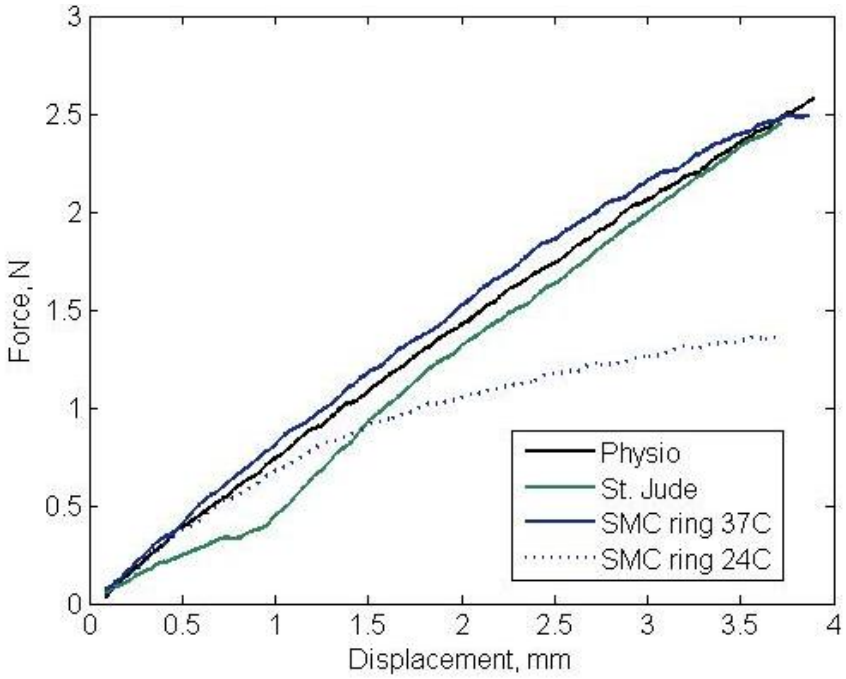


Figure 4.1 Compression test results for commercial rings and SMAC ring (37°C and 24°C).

Table 4.1 Static flow testing results from three individual explanted porcine hearts. Regurgitation is the backflow through the mitral valve.

Trial	1	2	3
Inner trigone distance (cm)	3.2	3.6	3.1
Anterior-Posterior (AP) distance (cm)	2.2	2.5	2.7
Maximum transverse distance (cm)	3.6	3.8	3.8
Regurgitation Failed valve (ml/min)	2275	716	533
Repair valve with activated ring (ml/min)	712	350	137
% Reduction after repair	68.7%	48.9%	25.7%

The hearts were similar in size, however, the amount of induced mitral regurgitation varied significantly between the hearts, Figure 4.2. All trials showed a decrease in MR after the valve was repaired and ring sutured into place.

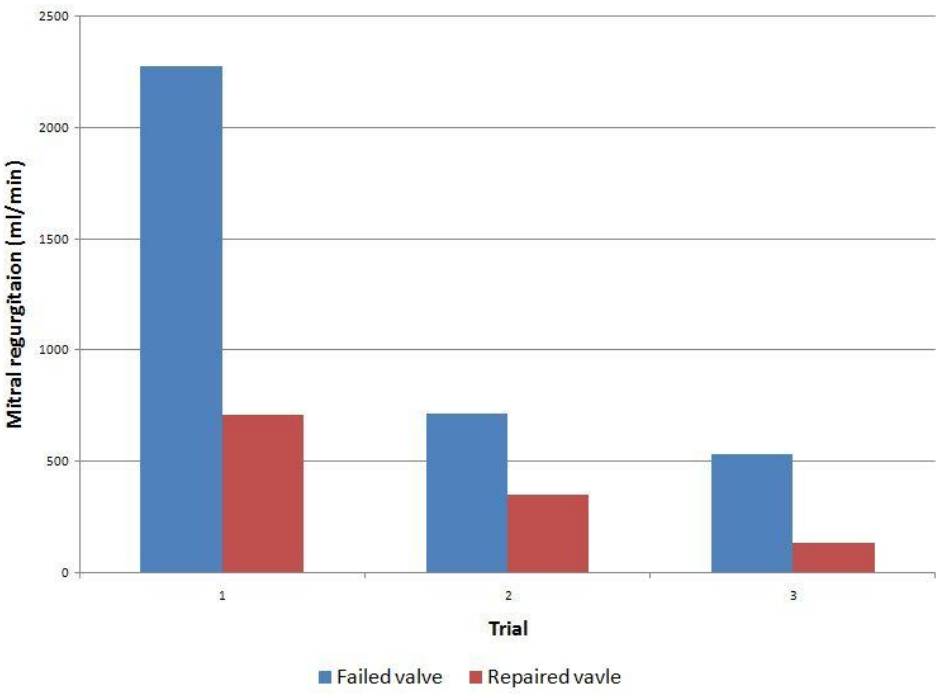


Figure 4.2 Mitral regurgitation of failed valve and repaired valve for each of the static flow trials

4.3 *Dynamic Flow Testing*

Mitral valve failed regurgitate fraction (FRF) was calculated as the percent difference between the failed valve output and baseline output measurements.

FRF = (baseline out – failed valve output)/baseline output)

Repaired regurgitant fraction (RRF) was calculated as the percent difference between repaired output and the baseline output.

RRF = (baseline output – repaired valve output)/baseline output

Percent regurgitant fraction data for each heart at both low and high left ventricular pressure is presented in Table 4.2.

A statistical model was developed to compare the effectiveness of the SMAC ring to the Physio ring. Several statistical approaches were considered. Models with factorial effects which parameterized the mean outflow at the two pressures (120 and 150 mm Hg), type of ring (Physio or SMAC) and status of valve (at failure or after repair) were not satisfactory because of the inhomogeneity of variance. The variability in mitral regurgitation is greater for the failed valves than the repaired valves, and no transformation of the data stabilized these variances, Figure 4.3. Volume data was normalized by the baseline measurements to eliminate the variation in the size of the hearts. It was found that the hearts that were randomly

Table 4.2 Regurgitant fraction for each heart at low and high peak left ventricular pressure. Percent regurgitant fraction is shown for both the failed valve (FRF) and the repaired valve (RRF), all hears had a decrease in MR after repair.

Heart	*Ring Type*	*Ring size (mm)*	*LV Pressure mm Hg*	*FRF (%)*	*RRF(%)*
1	Physio	26	120	46.9	17.7
			150	71.8	40.4
3	Physio	30	120	53.1	8.2
			150	74.9	35.1
4	Physio	31	120	22.1	14.5
			150	21.7	19.7
6	Physio	28	120	40.7	13.0
			150	46.7	17.6
8	Physio	26	120	35.1	13.2
			150	53.5	16.3
2	SMAC	26	120	20.5	17.9
			150	21.9	19.5
5	SMAC	26	120	25.8	14.1
			150	26.9	6.7
7	SMAC	30	120	16.9	3.1
			150	13.7	-6.9*
9	SMAC	26	120	39.0	16.9
			150	48.2	20.5
10	SMAC	26	120	51.6	22.7
			150	66.7	26.9

* indicated a valve that had a repaired regurgitant volume that was greater than the baseline measurement, possibly due to a natural defect.

assigned the Physio rings had lower baseline aortic output in all cases, Figure 4.4.

A mixed model using the RRF was fit to the data. The mixed model is an extension

of the generalized linear model (GLM) that allows for random effects. This type of model allowed for the random effects of the individual hearts (nested in the *ring type* factor) to be taken into consideration. The model parameters also included *ring type*, *pressure*, the crossed factors *pressure* and *ring type,* and random effects for the hearts (nested in the *ring type* factor). It was found that the RRF was positively associated with the FRF, indicating that degree of failure influenced repaired output. Therefore, in the statistical model the FRF was included as a covariate.

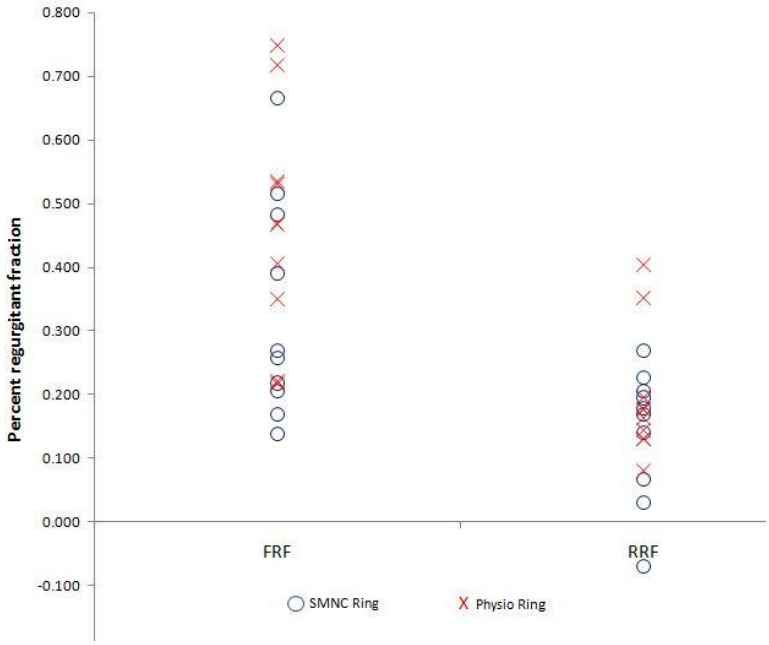


Figure 4.3 Regurgitant fraction for the output at both high and low left ventricular pressure for the Physio and the SMAC ring. The variability of the FRF is much greater than the variability of the RRF.

The model may be written as:

$$RRF = \mu + \alpha_i + \varphi_j + (\alpha\varphi)_{ij} + \beta FRF + H_{k(i)} + E_{ijk}$$

Where:

RRF = relative repaired regurgitant fraction

μ *= intercept term*

α_i *= ring type, i = 1,2 (SMAC or Physio)*

φ_j *= pressure, j=1,2 (120 or 150 mmHg)*

$(\alpha\varphi)_{ij}$ *= interaction of ring type and pressure*

β *= coefficient of the failed regurgitant fraction (FRF)*

FRF = failed regurgitant fraction

$H_{k(i)}$ *= heart effect term to account for variability between hearts*

E_{ijk} *= error term*

The heart effect term $H_{k(i)}$ and the error term E_{ijk} are random effects assumed normally distributed with constant variances. A statistical analysis was obtained using the MIXED procedure of the statistical software package SAS (SAS Institute, Incorporated, Cary NC), with the consultation of Dr. Jason Osborne. The ANOVA table, Table 4.3, quantifies the degree to which different factors in the model explain variability in RRF. A technical detail regarding the statistical inference is that since *ring type* was a "between heart" factor, an approximate F-test of no effect was constructed using an F-ratio with a denominator that was a linear combination of the

heart and error mean squares, and the reference sampling distribution used to compute a *p-value* was approximated using the Satterwaite approximation (with 14.6 denominator degrees of freedom). Diagnostic plots of residuals do not suggest any inhomogeneity of variance or non-normality of the repaired regurgitant fraction measurements, Figure 4.5 and Figure 4.6.

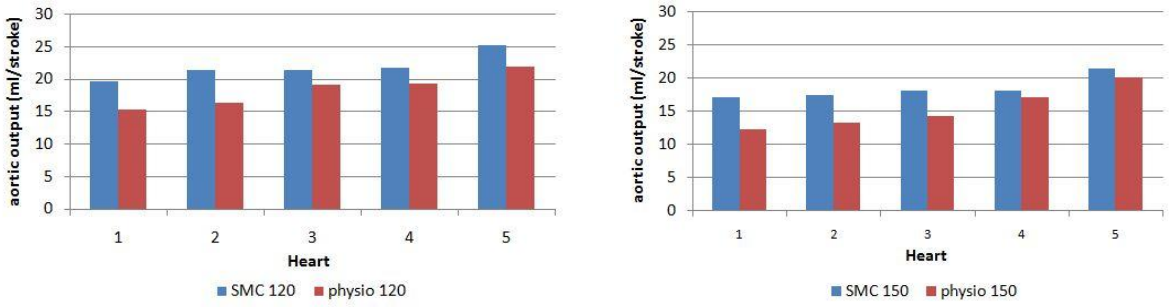


Figure 4.4 Baseline output per stroke per heart, (a) peak ventricular pressure 120 mm Hg, (b) peak ventricular pressure 150 mm Hg. Hearts that were randomly assigned the Physio ring had a lower baseline output measurement than hearts assigned the SMAC ring due to the natural size variation.

Table 4.3 ANOVA table for mixed model for RRF (repaired regurgitant fraction), the main source of error in the model is due to FRF and the random heart effect variables.

Source	Degrees of Freedom	Sum of squares (10^{-3})	Mean square (10^{-3})	*F*-ratio	*p*-value	Error degrees of freedom
Ring type	1	2.93	2.93	0.75	0.401	14.67
Pressure	1	0.53	0.53	0.24	0.641	7
*Pressure * Ring type*	1	4.73	4.73	2.14	0.187	7
FRF	1	19.05	19.49	8.59	0.022	7
Heart(ring type) between heart variable	8	61.81	7.73	3.48	0.059	7
Residual	7	15.52	2.217	-	-	-

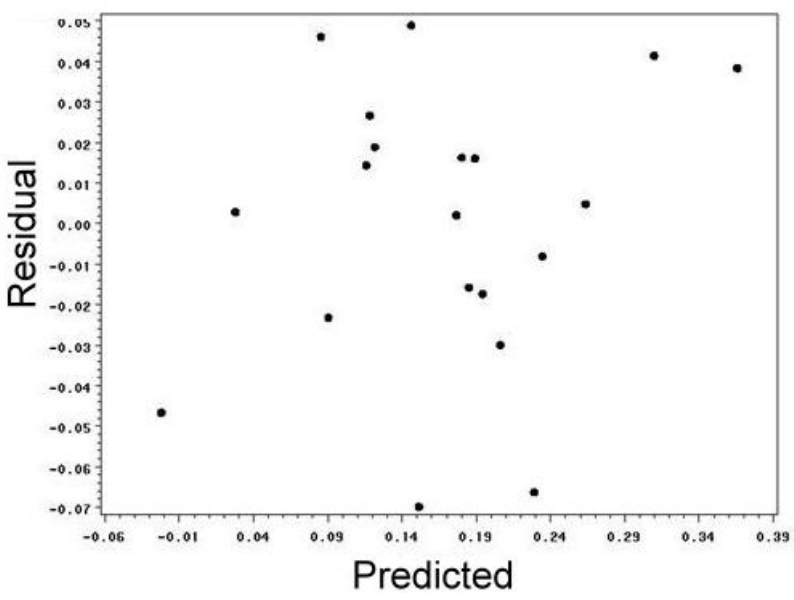


Figure 4.5 Residual plot data points are randomly distributed, therefore do not indicate any inhomogeneity of variance or non-normality of the RRF model

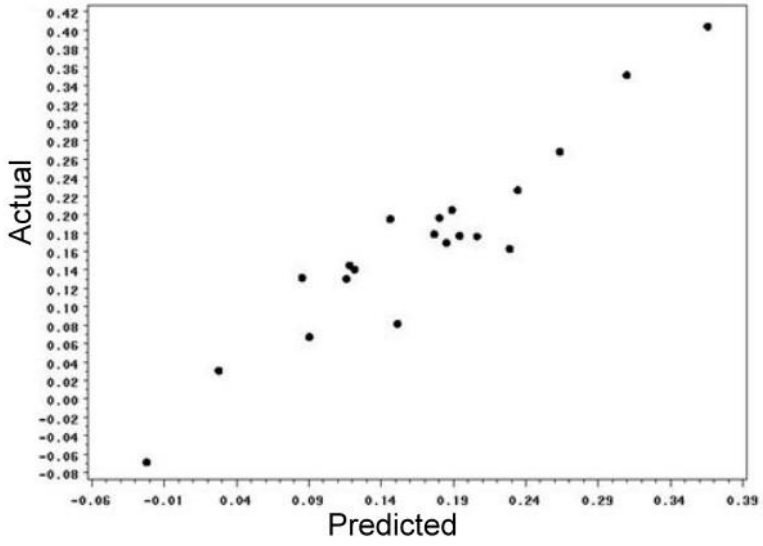


Figure 4.6 Actual versus predicted plot for the MIXED model for the RRF.

4.4 *Fatigue Testing*

Test data acquired from the first and the last cycles is shown are Figure 4.7. Two periods of data from selected cycles throughout the test are shown in Figure 4.8. No significant differences in force versus displacement characteristics can be observed from either plot. The minimum, maximum and average force was also plotted for every 1000 cycles, Figure 4.9. A statistical comparison of this data revealed no significant differences in mean force, minimum force and maximum force ($p < 0.05$).

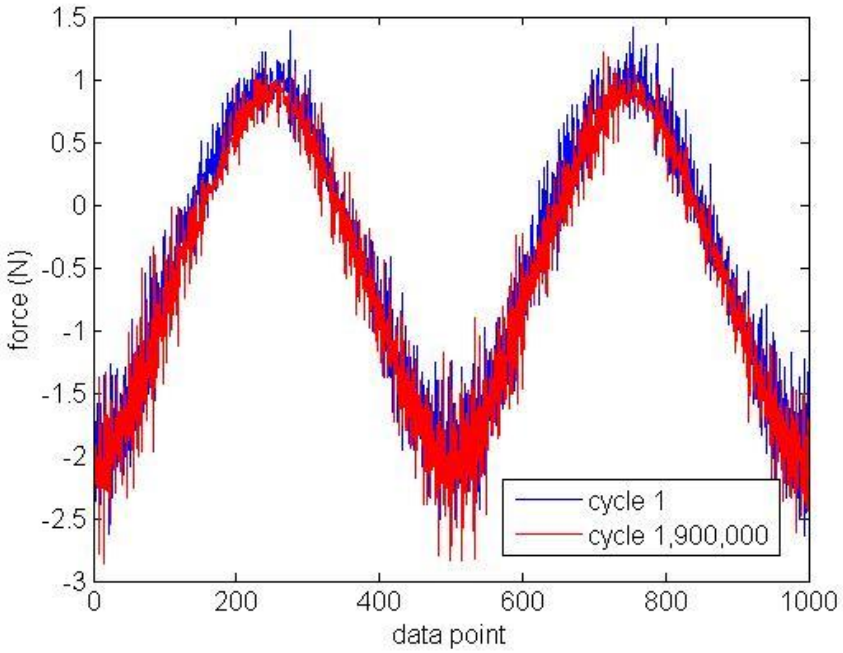


Figure 4.7 Two periods of fatigue test data: Cycle 1 versus Cycle 1.9 million.

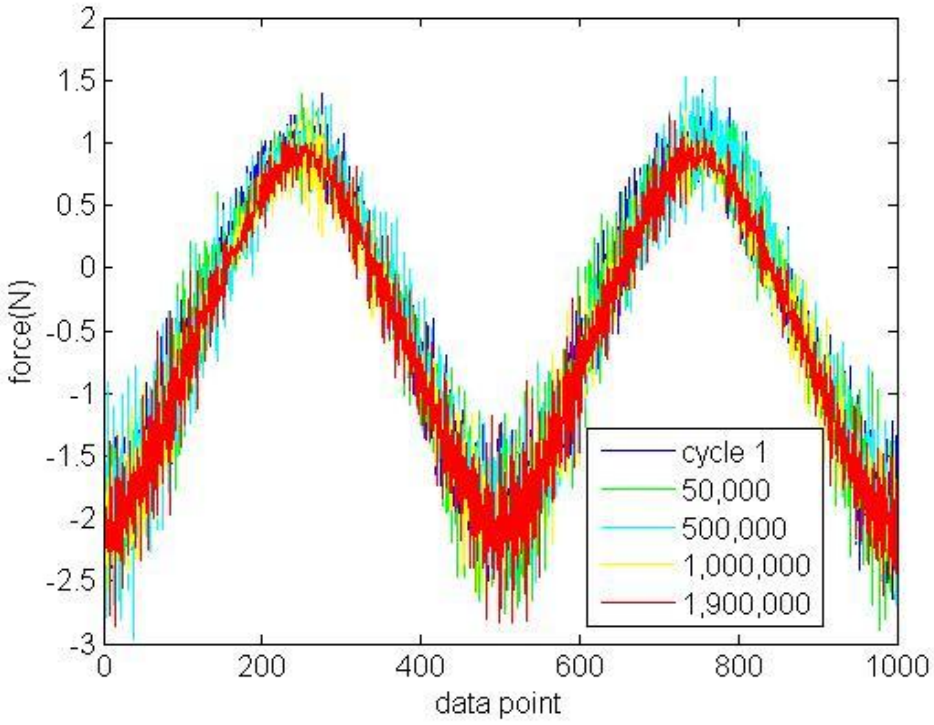


Figure 4.8 Several periods of force data over course of fatigue testing.

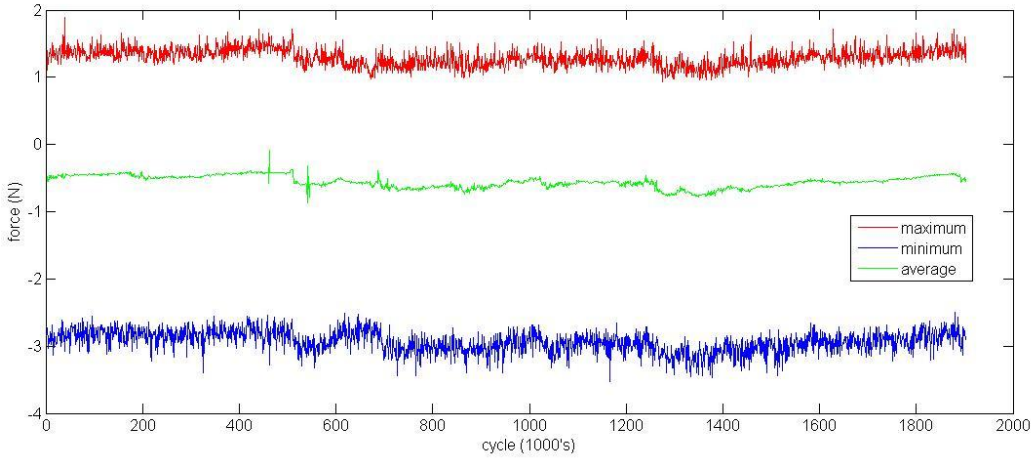
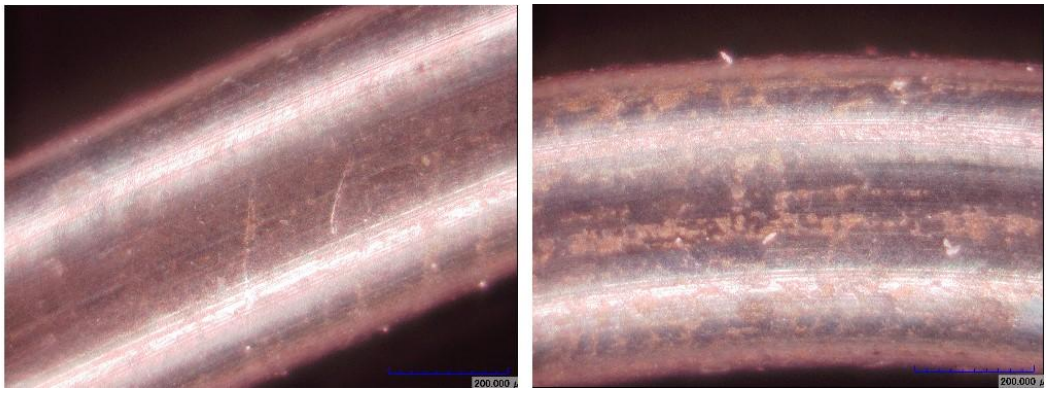


Figure 4.9 Maximum (tension) and minimum (compression) and mean force data over the 1.9 million cycles.

Micrographs were taken (Hirox Digital Microscope KH-7700, Hirox Co Ltd., River Edge, NJ) before (Figure 4.10) and after fatigue testing (Figure 4.11) to inspect for any defects or cracking. Images were taken at the maximum bend radius (the maximum strain point from ANSYS simulations) at magnifications up to 280x. The micrographs do not reveal any cracks or defects of the NiTi core. The NiTi did exhibit oxidation both before and after fatigue testing due to heat treatment being done in air.



a b

Figure 4.10 NiTi wire core before fatigue testing (280x magnification): (a) posterior section, (b) at trigone (maximum bend radius). Only surface oxidation and small surface scratches present.



a b

Figure 4.11 NiTi wire core after fatigue testing: (a) at 70x magnification showing silicone sheathing and wire core, (b) at 280x magnification showing maximum bend radius.

4.4.2 Confirmation of A_f temperature

Confirmation of A_f temperature was done by compressing the ring in the anterior-posterior direction while in a water bath at increasing temperatures using the same procedure previously mentioned. The results show that the A_f was unchanged (37°C) throughout fatigue testing.

4.5 *Robotic Manipulation*

The SMAC ring allowed for suture placement without tension on existing sutures or surrounding tissue, Figure 4.12 and Figure 4.13. The ductility of the SMAC ring allowed the ring to maintain its position without the constant aid of the robotic grips allowing the surgeon to have both robotic arms available for knot tying.

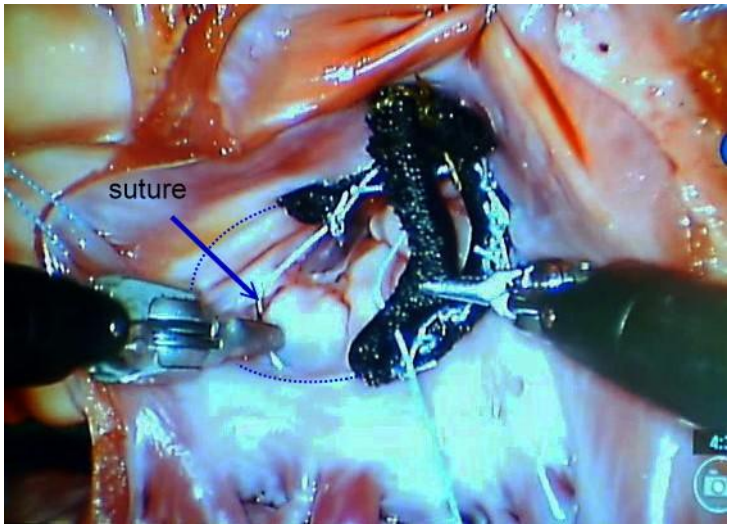


Figure 4.12 Robotic evaluation with SMAC ring, mitral annulus overlaid with dotted line. Half sutures in place, ring can be moved for visualization of annulus.



Figure 4.13 SMAC ring with only one stitch remaining, annulus is overlaid by dotted line.

The Physio ring recoiled sharply, and stress on the sutures caused significant deformation of the annular tissue, shown in Figure 4.14 and Figure 4.15.

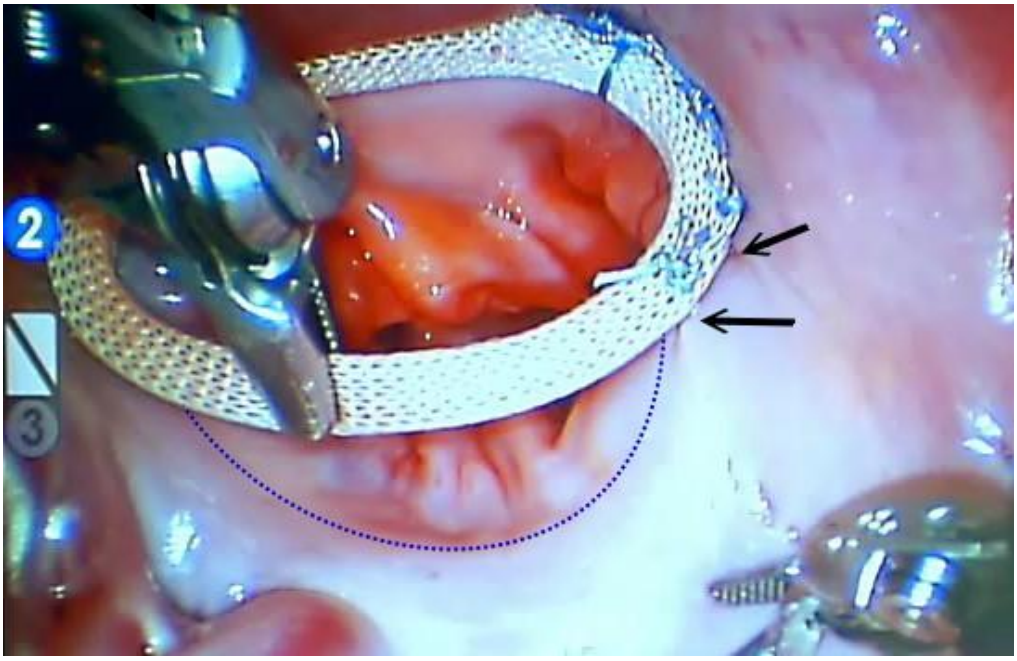


Figure 4.14 Robotic evaluation with Physio ring (Trial 3), dotted line shows the mitral annulus, arrows indicate areas of excessive stress on tissue and suture after 4th suture.

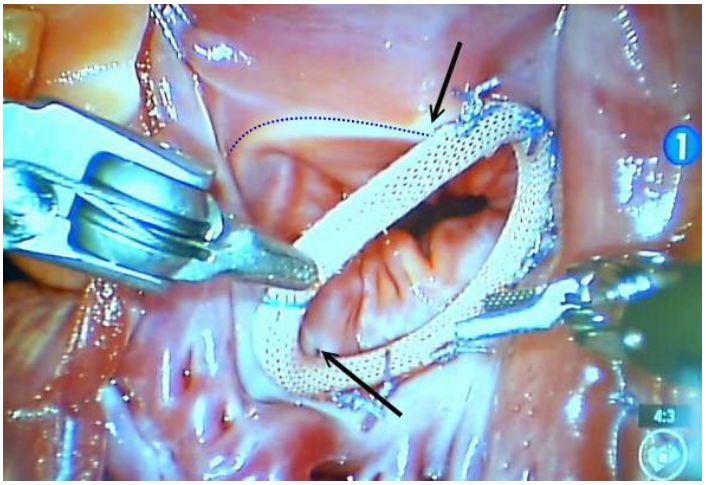


Figure 4.15 Physio ring with half of the sutures in place, dotted line outlines annulus, arrows indicate tissue deformation and stress on sutures.

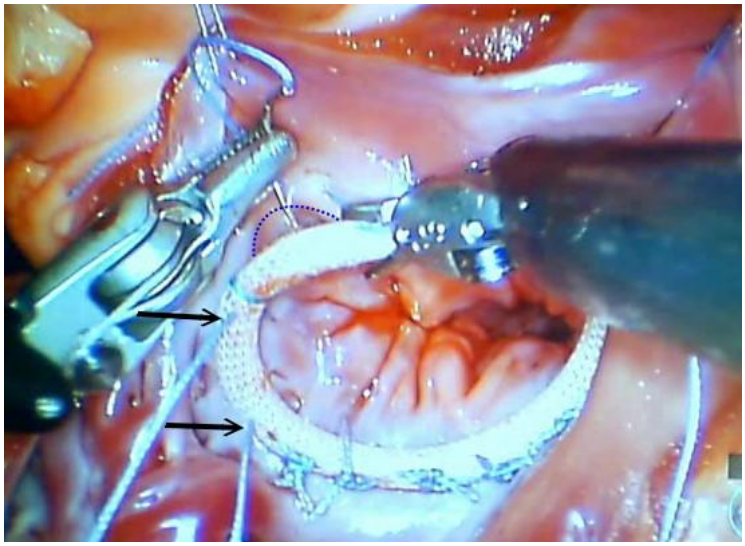


Figure 4.16 Physio ring with two more sutures to be placed, dotted line outlines annulus, arrows indicated un-knotted sutures.

In Trial 3 using the Physio ring, the last three sutures could not be knotted as they were placed, because of limited visibility of the annulus, Figure 4.16. As a comparison, the SMAC ring was sutured with the same method and all sutures were able to be knotted as soon as they were placed.

Chapter 5 Discussion and Conclusion

5.1 *Mechanical Testing*

The mechanical testing indicated that the ring should remain flexible during introduction and suturing, then transform into the austenitic state that has similar mechanical properties as other semi-rigid rings. Based on the mechanical compression testing the SMAC ring in its austenitic state (37°C) had comparable mechanical properties to the two commercial semi-rigid rings

5.2 *Static Pressure Testing*

Static pressure testing demonstrated that the SMAC ring was able to reduce mitral valve regurgitation in all trials. There was minimal leakage of the valve after repair caused by the suture holes, which in a dead heart do not heal. The percent reduction of mitral regurgitation is greater for valves that were more severely damaged, although the actual regurgitation volume is still greater. The variation in the degree of failure cannot be controlled; the cutting of the chordae tendinae will result in different failure for each heart due to the unique anatomy.

During the static pressure testing, it was determined that the SMAC ring size, which was based on average human anatomy, was larger than optimal for the

porcine hearts used in the surgical evaluations. Subsequent measurements of several explanted hearts from 70-100 kg swine were taken to determine the optimal ring dimensions for the porcine model. The ring sizes, 26 to 30 mm, were determined to accommodate the variation in porcine hearts.

During surgical evaluations associated with static pressure tests, the electrical supply wires used for ring activation were found to interfere with the surgical instruments as well as the surgeon's visibility. Therefore activation in subsequent studies used heated (37°C) saline solution.

5.3 *Dynamic Flow Testing*

ANOVA data showed that much of the variability is explained by the degree to which the valve was damaged, FRF. Mitral valve output varies depending on the pressure, and this difference was accounted for by taking all measurements at both pressures and using the pressure specific outflow measurements. Results showed no evidence of any effect due to ring type or pressure. Formal tests of no effect were not rejected at levels of significance of 0.17 or smaller. Both the Physio and the SMAC ring were able to reduce the mitral regurgitation; there was no significant difference in the repaired regurgitant fraction between the rings. Based on the dynamic flow testing, the mitral regurgitation repair is comparable between the Physio semi-rigid ring and the SMAC ring.

5.4 *Fatigue Testing*

Fatigue testing of the SMA did not reveal any significant changes in material properties, or result in any cracks or changes in the transformation temperature. NiTi fatigue is dependent on the material composition and processing history, therefore these results are specific to this material. Based on these results the SMA ring shows promise as a safe, durable ring for annuloplasty repair.

5.5 *Robotic Manipulation*

Dr. Cook commented that the SMAC ring in its martensitic phase was easily manipulated using the da Vinci robot. His surgical assessment of the Physio ring was that manipulation became more difficult generally after the fourth suture.

Two robotically trained cardiothoracic surgeons commented that the advantage of the SMAC ring is that it has the same final mechanical properties as semi-rigid rings, and can be easily introduced and manipulated with the robotic instruments. The difficulty of using a semi-rigid ring was demonstrated by the robotic handling evaluations conducted by Dr. Cook. He commented that the stiffness of the semi-rigid Physio ring prevented clear visualization of the annulus which presented difficulty in placing the sutures. Dr. Bolotin commented in the preliminary trials that the flexibility in the martensite phase made the ring easy to maneuver with the robotic instrument. Both surgeons agreed that this type of two-

phase ring would provide an advantage to robotic mitral valve repair. Overall, the subjective surgical assessment of the SMAC ring was that it was easy to manipulate, allowed for excellent visualization during suture placement, and placed minimal tension on the surrounding tissue and suture.

5.6 *Limitations*

One limitation of the SMAC ring is that its fabric sheath is not FDA and ISO 10993 certified biocompatible. Biocompatibility was not a concern for the explanted porcine heart trials conducted here; however future live animal trials and clinical trials will require a certified material. The explanted porcine hearts used in both the static pressure and dynamic flow test were freshly obtained; however, the tissue compliance is notably different from live hearts. No sterilization of the SMAC ring was completed during these trials. An assumption of this research was that a suitable sterilization method would be able to achieve acceptable properties. Several sterilization methods for NiTi biomedical devices have been studied by Shabalovaky (1996), based on this research either autoclaving or boiling in water produced NiTi with acceptable sterilization levels and surface characteristics (S. A. Shabalovskaya, 1996). All *in vitro* experiments have to make assumptions and are simply models of an actual system. The evaluation presented in this research were completed in order to establish the feasibility of the proposed approach and to evaluate its relative strengths and weaknesses.

5.7 *Conclusions*

Over the last decade, advances in closed-chest cardiopulmonary bypass, cardioplegic arrest methods, voice controlled endoscopes, and three-dimensional visualization has lead to an increase in minimally invasive cardiac procedures (Kypson & Chitwood, 2004). Today, an increasing number of surgeons routinely perform minimally invasive mitral valve repair (A. P. Kypson & Chitwood, 2004).

The ability of the SMAC ring to fit through the trocar will allow an alternative to flexible rings for totally endoscopic mitral valve repair. The SMAC ring has the potential to satisfy the need for a semi-rigid ring in robotic mitral valve repair. Current semi-rigid rings cannot fit through the 8mm trocars. In addition, semi-rigid rings are generally avoiding in minimally invasive surgery due to the difficulty of maneuvering the ring in the confined space of the left atrium with the robotic instruments. This research demonstrates that the SMAC ring can be an alternative to flexible rings in robotic mitral valve repair. The SMAC ring has similar mechanical characteristics to semi-rigid rings once deployed. The decrease in mitral regurgitation in both the static pressure and dynamic flow testing was comparable using the SMAC ring to the Physio ring. Cyclic fatigue testing has demonstrated that the ring can withstand the cyclic movement of the mitral annulus during the cardiac cycle. The SMAC was deployed through a trocar. When sutured into place with robotic instruments there was reduced tension on the suture and deformation of

surrounding tissue. The surgical assessment of the SMAC ring was that it provided excellent visualization of the annulus, and was easily maneuvered with the robotic instruments. These evaluations have shown that the SMAC ring has the potential to provide surgeons a viable alternative to flexible rings when performing minimally invasive robotic mitral valve repair.

Chapter 6 Future Research

In order to further evaluate the SMAC ring, additional testing will be required. These include *in vivo* animal testing and tests for premarket clinical trials outlined in the Guidance for Annuloplasty Rings 510(k) Submissions (U.S. Food and Drug Administration Center for Device and Radiological Health, 2001).

6.1 *Animal Testing*

The *in vitro* evaluations thus far have been invaluable to the design of the SMAC ring, baseline comparisons with other commercial rings, and overall assessment of the ring using robotic instruments. The next step is *in vivo* animal testing. *In vivo* animal testing is used to evaluate surgical handling, hemodynamics and pathology. Animal testing is expensive and time consuming; therefore it was imperative that the ring design be finalized before animal testing. Animal testing is not feasible for long term durability studies, however, insight into biocompatibility and potential side effects can be gained.

Cardiac valve implant standard assessments have been established by the International Organization for Standardization in CV5840-2005 (Cardiovascular implants – Cardiac valve prostheses). The document describes all aspects of testing that are required to be completed before clinical trials can be considered.

The device tested must be identical to the device intended for clinical use, including parameters such as size, design, materials and sterilization method. The surgical procedure (suture technique and the location and orientation of the implant device) must also be defined and repeatability must be ensured. At least six animals of the same species, preferably of the same sex and age, must be implanted with the device for a minimum of 20 weeks. A control group consisting of at least two animals should be implanted with a similar approved device. The proposed study would involve a minimum of eight animals; six would undergo CPB and be implanted with a SMAC ring. The remaining two animals would comprise the control group, and be implanted with a Physio ring. Hemodynamic performance evaluations need to be performed; at a minimum this should include measurement of the pressure gradient across the valve, resting cardiac output, and any regurgitation. Pathology evaluation should include assessment of major organs, signs of thrombosis, and structural evaluation of the device.

The ISO 5840-2005 documentation also details the requirements for official reporting of the results. A medical pre-assessment of each animal should be included with information of the size, weight, breed and sex of the animal. Blood testing both before and after the procedure should be included. A detail of the surgical procedure should be included, along with all medication administered. The report should contain a surgical assessment of the device including the surgical handling characteristics, and a discussion of the unique attributes of the device. The

detailed results of all hemodynamic studies will be reported. The pathology report should include both a gross and microscopic report for all animals including those that did not survive for the trial period. For those animals that did not survive through the trial, cause of death should be established and investigated to determine if it is device related. Device examination should include *in situ* examination for evidence of thrombosis, as well as an explantation study of the device for any structural breakage or changes.

The proposed animal testing should utilize porcine or small breed sheep. Both animals have hearts that are anatomic and physiologic similar to humans, are readily available at a relatively low cost and have hemodynamic values that are similar to humans (Bianco et al., 2004; Kunzelman, Cochran, Verrier, & Eberhart, 1994). A drawback to using porcines in animal trials is they tend to have an increased chronic tissue response, and therefore are not a representative model in accessing thrombogenicity of a cardiac implant (Bianco et al., 2004). Accordance with the Guide for the Care and Use of Laboratory Animals (NIH 1985) should be strictly followed.

Hemodynamic performance should be assessed by transthoracic echocardiography, which should be done before surgery to establish a baseline, one week after, and monthly up to the end of the trial. Specifically, the echocardiogram should note any mitral stenosis, regurgitation, irregular leaflet coaptation and valve

function, and any ring interference or dehiscence. Animals should also be monitored for any infection, endocarditis, or abnormalities. Animals should be humanely euthanized at end of the 20 weeks. Pathological gross evaluations should include mitral annulus condition, measurement of orifice area, leaflet mobility, fibrous tissue growth, and condition of the ring. Ring adherence, position and any structural changes or defects should also be evaluated. Histological samples of the annulus, leaflets and adjacent tissue of the left atrium and ventricle would evaluate any fibrous tissue, leaflet thickening, thrombus formation and necrosis. Statistical comparisons between the Physio and SMAC ring of all data should be used to determine any difference between rings. Surgical assessment and comparison of the handling characteristics of the two rings should be included in the report.

6.2 *FDA 510(k) Guidance*

The FDA Guidance for Annuloplasty Rings 510(k) Submissions was developed when annuloplasty rings were reclassified from Class III to Class II with special controls device. Manufacturers of new annuloplasty rings are required to demonstrate that their new device is substantially equivalent to an existing approved ring. Several performance tests are outlined: biocompatibility testing, computational structural analysis, tensile testing, suture pull-out testing, sterilization validation, biological testing including bioburden and pyrogen testing, and shelf-life validation.

6.2.1 Biocompatibility

The materials of the SMAC ring (NiTi, silicone and polyester) have previously undergone biocompatibility testing in accordance with the FDA biocompatibility guidance: Use of International Organization for Standardization (ISO) 10993 'Biological Evaluation of Medical Devices Part 1: Evaluation and Testing'. The standard includes tests for biocompatibility, hemocompatibility and hemolysis. The polyester material used for the sewing cuff was not certified by the supplier to meet FDA and ISO 10993 biocompatibility standards. For the purpose of this study, the certified material could not be cost justified, however, it is similar to other approved polyester material. Future SMAC rings used in testing should use certified material. Biocompatibility testing minimized the potential for developing thrombosis, tissue and blood damage, and endocarditis.

6.2.2 Structural Analysis

Structural analysis is suggested to prevent fracture of the core of the ring. The FDA guidelines suggest both a finite element analysis as well as tensile testing to prevent failure. Tensile testing is suggested to ensure that the ring will not fail at loads greater than loads that would be experienced *in vivo*; however, no guidance of the magnitude of the load is given. The cyclical fatigue testing and ANSYS modeling previously presented was conducted at a displacement that was greater than normal

in vivo values. An additional tensile test to failure should also be conducted to quantify the load at which the ring would actual fail.

6.2.3 Suture Pull-out Tests

A concern with annuloplasty rings is the potential for thrombosis and thromboembolisms which can be caused by any loose or frayed thread, material or suture. The potential for ring dehiscence due to failure of the sewing ring fabric and seam is another risk. Suture pull out tests and tensile testing of the fabric are suggested to minimize these risks.

6.2.4 Sterilization Validation

Sterilization validation is suggested to reduce the risk of endocarditis. The sterilization process should be able to met the Sterilization Assurance Limit of 10^{-6}, outlined in "510(k) Sterility Review Guidance K90-1". Future research would need to include investigation of various sterilization methods and the possible effects on the mechanical properties of NiTi. Good surface condition of NiTi has been achieved with the sterilization methods of autoclaving and boiling in water (S. A. Shabalovskaya, 1996). Sterilization of NiTi has been shown to change the oxide thickness; both ethylene oxide (EtO) and steam autoclaving have been shown to increase the oxide layer (S. A. Shabalovskaya, 2002). EtO, steam and dry heat have all been shown to increase the Ni concentration on the surface, which would

decrease the biocompatibility of NiTi (S. A. Shabalovskaya, 2002). Shabalovskaya et al. have shown that chemical etching in an HF/HNO_3 solution to remove surface oxidation, then boiling in water resulted in lower Ni surface concentrations and a homogeneous TiO_2 layer. The resulting NiTi material had increased biocompatibility and corrosion resistance (S. A. Shabalovskaya, 1995).

6.2.5 Bioburden and Pyrogen testing

Endocarditis is an infection of the heart caused by bacteria which is a serious risk to valve repair patients. Both bioburden and pyrogen testing are designed to minimize the risk. Bioburden is done before sterilization to determine type and quantity of bacteria that are present on the device. These usually come from the manufacturing process or the materials. Pyrogen (induction of a fever) testing is another test to determine the level of contaminants; it is usually done after sterilization.

6.2.6 Shelf-life validation

Shelf-life validation is to ensure the product does not contain any contaminants when the product is ultimately used. Packaging, which provides a barrier to contamination, is considered in shelf-life validation. Shipping and storage conditions are simulated to evaluate shelf-life under variations in temperature, humidity, and atmospheric pressure.

6.3 *Summary*

Overall, the additional tests outlined will position the SMAC ring for FDA 510(k) premarket approval and clinical trials. In the near future, improved visualization methods, real-time tactile feedback, smaller instrument size and greater variety of end efforts will be developed enabling more complex surgeries to be completed robotically (A. P. Kypson & Chitwood, 2004). New technological advances combined with the growth of trained surgeons will continue to increase the number of robotic mitral valve repairs performed every year. The SMAC ring will offer the mechanical advantages of semi-rigid rings, combined with the insertion and manipulation performance of flexible rings, providing surgeons with an alternative to flexible rings.

REFERENCES

Arita, M., Kasegawa, H., & Umezu, M. (2004). Static analysis of annuloplasty rings sutured on an annulus model of the mitral valve: Comparison between the Duran ring and the Carpentier Classic ring. *Journal of Artificial Organs, 7*(1), 30-36.

Ballantyne, G. H. (2002). Robotic surgery, telerobotic surgery, telepresence, and telementoring. Review of early clinical results. *Surgical Endoscopy, 16*(10), 1389-1402.

Bianco, R. W., Grehan, J. F., Grubbs, B. C., Mrachek, J. P., Schroeder, E. L., Schumacher, C. W., et al. (2004). Large animal models in cardiac and vascular biomaterials research and testing. In B. D. Ratner, A. S. Hoffman, F. J. Schoen & J. E. Lemons (Eds.), *Biomaterials science: An introduction to materials in medicine* (2nd ed., pp. 379-395). San Diego, CA: Elsevier Academic Press.

Carpentier, A. (1976). Congenital malformations of the mitral valve in children. pathology and surgical treatment. *Journal of Thoracic and Cardiovascular Surgery, 72*(6), 854.

Carpentier, A. (2007). The surprising rise of nonthrombogenic valvular surgery. *Nature Medicine, 13*, 1165-1168.

Casselman, F. P., Van Slycke, S., Wellens, F., De Geest, R., Degrieck, I., Vermeulen, Y., et al. (2003). From classical sternotomy to truly endoscopic mitral valve surgery: A step by step procedure. *Heart, Lung & Circulation, 12*(3), 172-177.

Cohn, L. H., & Edmunds, L. H.,Jr (Eds.). (2007). *Cardiac surgery in the adult* (3rd ed.). New York: McGraw-Hill Medical.

Cohn, L. H., Adams, D. H., Couper, G. S., Bichell, D. P., Rosborough, D. M., Sears, S. P., et al. (1997). Minimally invasive cardiac valve surgery improves patient satisfaction while reducing costs of cardiac valve replacement and repair. *Annals of Surgery, 226*(4), 421-6; discussion 427-8.

Cosgrove, D. M.,3rd, Arcidi, J. M., Rodriguez, L., Stewart, W. J., Powell, K., & Thomas, J. D. (1995). Initial experience with the Cosgrove-Edwards annuloplasty system. *The Annals of Thoracic Surgery, 60*(3), 499-503; discussion 503-4.

Dagum, P., Timek, T., Green, G. R., Daughters, G. T., Liang, D., Ingels, N. B.,Jr, et al. (2001). Three-dimensional geometric comparison of partial and complete flexible mitral annuloplasty rings. *The Journal of Thoracic and Cardiovascular Surgery, 122*(4), 665-673.

Dauskardt, R. H., Duerig, T. W., & Ritchie, R. O. (1989). Effects of *in situ* phase transformation on fatigue-crack propagation in titanium-nickel shape-memory alloys. *MRS International Meeting on Advanced Materials,* Pittsburgh, PA. 243-249.

David, T. E., Komeda, M., Pollick, C., & Burns, R. J. (1989). Mitral valve annuloplasty: The effect of the type on left ventricular function. *The Annals of Thoracic Surgery, 47*(4), 524-7; discussion 527-8.

Duran, C. M. (1999). Surgical techniques for the repair of anterior mitral leaflet prolapse. *Journal of Cardiac Surgery, 14*(6), 471-481.

Edwards Lifesciences LLC. (2005a). *Carpentier-Edwards Classic annuloplasty system brochure* Retrieved February 9, 2009 from (http://www.edwards.com/products/rings/classic.htm ed.) edwards.com.

Edwards Lifesciences LLC. (2005b). *Carpentier-Edwards Physio annuloplasty ring brochure* Retrieved February 9, 2009 from (http://www.edwards.com/products/rings/physio.htm ed.) edwards.com.

Edwards Lifesciences LLC. (2005c). *Cosgrove-Edwards annuloplasty system brochure* Retrieved February 9, 2009 from (http://www.edwards.com/products/rings/cosgrove.htm ed.)

Es-Souni, M., Es-Souni, M., & Fischer-Brandies, H. (2005). Assessing the biocompatibility of NiTi shape memory alloys used for medical applications. *Analytical and Bioanalytical Chemistry, 381*(3), 557-567.

Fasol, R., Meinhart, J., Deutsch, M., & Binder, T. (2004). Mitral valve repair with the Colvin-Galloway Future band. *The Annals of Thoracic Surgery, 77*(6), 1985-8; discussion 1988.

Felger, J. E., Chitwood, W. R.,Jr, Nifong, L. W., & Holbert, D. (2001). Evolution of mitral valve surgery: Toward a totally endoscopic approach. *The Annals of Thoracic Surgery, 72*(4), 1203-8; discussion 1208-9.

Flachskampf, F. A., Chandra, S., Gaddipatti, A., Levine, R. A., Weyman, A. E., Ameling, W., et al. (2000). Analysis of shape and motion of the mitral annulus in subjects with and without cardiomyopathy by echocardiographic 3-dimensional reconstruction. *Journal of the American Society of Echocardiography : Official Publication of the American Society of Echocardiography, 13*(4), 277-287.

Food and Drug Administration. (2002). In Center for Devices and Radiological Health (Ed.), *510(k) Summary for SJM Seguin annuloplasty ring*

Gillinov, A. M., Cosgrove, D. M., Blackstone, E. H., Diaz, R., Arnold, J. H., Lytle, B. W., et al. (1998). Durability of mitral valve repair for degenerative disease. *The Journal of Thoracic and Cardiovascular Surgery, 116*(5), 734-743.

Glower, D. D., Landolfo, K. P., Clements, F., Debruijn, N. P., Stafford-Smith, M., Smith, P. K., et al. (1998). Mitral valve operation via port access versus median sternotomy. *European Journal of Cardio-Thoracic Surgery : Official Journal of the European Association for Cardio-Thoracic Surgery, 14 Suppl 1*, S143-7.

Goodman, L. R., Kay, H. R., Teplick, S. K., & Mundth, E. D. (1983). Complications of median sternotomy: Computed tomographic evaulation. *American Journal of Roentgenology, 141*(2), 225-230.

Hartrumpf, M., Stock, U. A., Kuehnel, R. U., & Albes, J. M. (2006). Fracture of Colvin-Galloway Future band causing a tear in the anterior mitral leaflet. *The Annals of Thoracic Surgery, 81*(5), 1879-1880.

Kaplan, S. R., Bashein, G., Sheehan, F. H., Legget, M. E., Munt, B., Li, X. N., et al. (2000). Three-dimensional echocardiographic assessment of annular shape changes in the normal and regurgitant mitral valve. *American Heart Journal, 139*(3), 378-387.

Kunzelman, K. S., Cochran, R. P., Verrier, E. D., & Eberhart, R. C. (1994). Anatomic basis for mitral valve modelling. *The Journal of Heart Valve Disease, 3*(5), 491.

Kypson, A. P., & Chitwood, W. R.,Jr. (2004). Robotic mitral valve surgery. *American Journal of Surgery, 188*(4A Suppl), 83S-88S.

Kypson, A. P. (2003). Robotic cardiac surgery. *Journal of Long-Term Effects of Medical Implants, 13*(6), 451.

Losanoff, J. E., Richman, B. W., & Jones, J. W. (2002). Disruption and infection of median sternotomy: A comprehensive review. *European Journal of Cardio-Thoracic Surgery, 21*, 831-839.

McKelvey, A. L., & Ritchie, R. O. (1999). Fatigue-crack propagation in nitinol, a shape-memory and superelastic endovascular stent material. *Journal of Biomedical Materials Research, 47*(3), 301-308.

Medtronic, Inc. (a) *CG Future® ring and band system brochure.* Retrieved February 17, 2009, from http://www.medtronic.com/your-health/heart-valve-disease/about-surgery/our-heart-valve-products/cg-future-ring-band/index.htm

Medtronic, Inc. (b). *Duran AnCore ring and band system brochure.* Retrieved February 17, 2009, from http://www.medtronic.com/your-health/heart-valve-

disease/about-surgery/our-heart-valve-products/duran-ancore-ring-band/index.htm

Mehmanesh, H., Henze, R., & Lange, R. (2002). Totally endoscopic mitral valve repair. *Journal of Thoracic and Cardiovascular Surgery, 123*, 96-97.

National Library of Medicine and the National Institutes of Health Medline Plus Medical Encyclopedia. (2006). *Mitral valve prolapse.* Retrieved February 17, 2009, from http://www.nlm.nih.gov/medlineplus/ency/imagepages/18148.htm

National Library of Medicine and the National Institutes of Health Medline Plus Medical Encyclopedia. (2008a). *Heart section through middle.* Retrieved February 17, 2009, from http://www.nlm.nih.gov/medlineplus/ency/imagepages/1056.htm

National Library of Medicine and the National Institutes of Health Medline Plus Medical Encyclopedia. (2008b). *Heart, front view.* Retrieved February 17, 2009, from http://www.nlm.nih.gov.www.lib.ncsu.edu:2048/medlineplus/ency/imagepages/1097.htm

Nishida, M., Wayman, C., & Honma, T. (1986). Precipitation processes in near-equiatomic TiNi shape memory alloys. *Metallurgical and Materials Transactions A, 17*(9), 1505-15015.

Okada, Y., Shomura, T., Yamaura, Y., & Yoshikawa, J. (1995). Comparison of the Carpentier and Duran prosthetic rings used in mitral reconstruction. *The Annals of Thoracic Surgery, 59*(3), 658-662.

Pellerin, D., Brecker, S., & Veyrat, C. (2002). Degenerative mitral valve disease with emphasis on mitral valve prolapse. *Heart (British Cardiac Society), 88 Suppl 4*, iv20-8.

Pelton, A. R., Russell, S. M., & DiCello, J. (2003). The physical metallurgy of nitinol for medical applications. *JOM Journal of the Minerals, Metals and Materials Society, 55*(5), 33-37.

Raffoul, R., Uva, M. S., Rescigno, G., Belli, E., Scorsin, M., Pouillart, F., et al. (1998). Clinical evaluation of the Physio annuloplasty ring. *Chest, 113*(5), 1296-1301.

Ramaiah, K. V., Saikrishna, C. N., & Bhaumik, S. K. (2005). Processing of Ni-Ti shape memory alloy wires. *International Conference on Smart Materials Structures and Systems,* Bangalore, India. 141-147.

Richards, A., Cook, R., Bolotin, G., & Buckner, G. (2009). A dynamic heart system to facilitate the development of mitral valve repair techniques. *Annals of Biomedical Engineering,* doi:10.1007/s10439-009-9653-x.

Rubenstein, F., Reichart, B., & Letsou, G. (2001). Alternatives in selection of rings for mitral annuloplasty. *Current Opinion in Cardiology, 16*, 136-139.

Salgo, I. S., Gorman, J. H.,3rd, Gorman, R. C., Jackson, B. M., Bowen, F. W., Plappert, T., et al. (2002). Effect of annular shape on leaflet curvature in reducing mitral leaflet stress. *Circulation, 106*(6), 711-717.

Seguin, J. R., Demaria, R., Rogier, R., & Chaptal, P. A. (1996). Advance in mitral valve repair using a device flexible in three dimensions. the St. Jude Medical-Seguin annuloplasty ring. *ASAIO Journal (American Society for Artificial Internal Organs : 1992), 42*(5), M368-71.

Shabalovskaya, S. A. (2002). Surface, corrosion and biocompatibility aspects of nitinol as an implant material. *Bio-Medical Materials and Engineering, 12*, 69-109.

Shabalovskaya, S. A. (1995). Surface spectroscopic characterization of TiNi nearly equiatomic shape memory alloys for implants. *Journal of Vacuum Science Technology. A. Vacuum, Surfaces, and Films, 13*(5), 2624.

Shabalovskaya, S. A. (1996). On the nature of the biocompatibility and on medical applications of NiTi shape memory and superelastic alloys. *Bio-Medical Materials and Engineering, 6*(4), 267-289.

Sharony, R., Saunders, P. C., Nayar, A., McAleer, E., Galloway, A. C., Delianides, J., et al. (2004). Semirigid partial annuloplasty band allows dynamic mitral annular motion and minimizes valvular gradients: An echocardiographic study. *The Annals of Thoracic Surgery, 77*(2), 518-22; discussion 522.

Spiegelstein, D., Ghosh, P., Sternik, L., Tager, S., Shinfeld, A., & Raanani, E. (2007). Current strategies of mitral valve repair. *The Israel Medical Association Journal : IMAJ, 9*(4), 303-309.

St. Jude Medical, I. (a). *SJM seguin semi-rigid .* Retrieved February 1, 2009. from http://www.sjm.com/devices/device.aspx?name=SJM+Seguin+Semi-Rigid+Ring&type=23&location=us

St. Jude Medical, I. (b). *SJM tailor flexible ring + band.* Retrieved February 17, 2009, from http://www.sjm.com/devices/device.aspx?name=SJM+Tailor+Flexible+Ring+%2b+Band&type=23&location=us

Tatooles, A. J., Pappas, P. S., Gordon, P. J., & Slaughter, M. S. (2004). Minimally invasive mitral valve repair using the da Vinci robotic system. *The Annals of Thoracic Surgery, 77*(6), 1978-82; discussion 1982-4.

TiNi Alloy Company, Inc. *Nitinol - NiTi shape memory alloy; high temperature phase.* Retrieved February 2009, from http://www.matweb.com/search/DataSheet.aspx?MatGUID=de9dd08433714f698d513766dccea437&ckck=1

Tobushi, H., Shimeno Y., & Hackisuka T., K. T. (1998). Influence of strain rate on superelastic properties of TiNi shape memory alloy. *Mechanics of Materials, 30*, 141-150.

Tolomeo, D., Davidson, S., & Santinoranont, M. (2001). Cyclic properties of superelastic nitinol: Design implications. *Proceedings of the Internationla Conference on Shape Memory and Superelastic Technologies,* 471.

U.S. Food and Drug Administration Center for Device and Radiological Health. (2001). *Guidance for annuloplasty rings 510(k) submissions; final guidance for industry and FDA staff* No. 1358)

U.S. Food and Drug Administration Center for Device and Radiological Health. (2009). *Manufacturere and user facility device experience database (MAUDE*

data). Retrieved February 1, 2006, from http://www.accessdata.fda.gov/scripts/cdrh/cfdocs/cfMAUDE/search.CFM

U.S. National Institutes of Health. (2008). *Safety and efficacy study of the Sorin 3D annuloplasty ring for mitral repair (MEMO3D).* Retrieved February 14, 2009, from http://clinicaltrials.gov/ct2/show/NCT00567853?term=MEMO+3D&rank=1

Wang, Z. G., Zu, X. T., Feng, X. D., Zhu, S., Zhou, J. M., & Wang, L. M. (2004). Annealing induced evolution of transformation characteristics of TiNi shape memory alloys. *Physica B, 353*, 9-14.

Weinberg, S., & King, M. W. (2004). Medical fibers and biotextiles. In B. D. Ratner, A. S. Hoffman, F. J. Schoen & J. E. Lemons (Eds.), *Biomaterials in science: An introduction to materials in medicine* (2nd ed., pp. 86). San Diego, CA: Elsevier, Inc.

Yeung, K. W. K., Cheung, K. M. C., Lu, W. W., & Chung, C. Y. (2004). Optimization of thermal treatment parameters to alter austenitic phase transition temperature of NiTi alloy for medical implant. *Materials Science and Engineering. A, 383*(2), 213-218.